ACS OMEGA

http://pubs.acs.org/journal/acsodf

Article

Aza-phenol Based Macrocyclic Probes Design for "CHEF-on" Multi Analytes Sensor: Crystal Structure Elucidation and Application in Biological Cell Imaging

Mohafuza Khatun, Pravat Ghorai, Jayanta Mandal, Sougata Ghosh Chowdhury, Parimal Karmakar, Salvador Blasco, Enrique García-España, and Amrita Saha*

Cite This: *ACS Omega* 2023, 8, 7479−7491

Read Online

ACCESS | Metrics & More | Article Recommendations | Supporting Information

ABSTRACT: Metal bound macrocyclic compounds found in biological systems inspired us to design and synthesize two Robson-type macrocyclic Schiff-base chemosensors, $\mathbf{H_2L1}$ ($\mathbf{H_2L1}$=1,11-dimethyl-6,16-dithia-3,9,13,19-tetraaza-1,11(1,3)-dibenzenacycloicosaphane-2,9,12,19-tetraene-1,11-diol) and $\mathbf{H_2L2}$ ($\mathbf{H_2L2}$=1,11-dimethyl-6,16-dioxa-3,9,13,19-tetraaza-1,11(1,3)-dibenzenacycloicosaphane-2,9,12,19-tetraene-1,11-diol). Both the chemosensors have been characterized with different spectroscopic techniques. They act as multianalyte sensor and exhibit "turn-on" fluorescence toward different metal ions in 1X PBS (Phosphate Buffered Saline) solution. In presence of Zn^{2+}, Al^{3+}, Cr^{3+} and Fe^{3+} ions, $\mathbf{H_2L1}$ exhibits ∼6-fold enhancement of emission intensity, while $\mathbf{H_2L2}$ shows ∼6-fold enhancement of emission intensity in the presence of Zn^{2+}, Al^{3+} and Cr^{3+} ions. The interaction between the different metal ion and chemosensor have been examined by absorption, emission, and ^{1}H NMR spectroscopy as well as by ESI-MS$^+$ analysis. We have successfully isolated and solved the crystal structure of the complex $[Zn(\mathbf{H_2L1})(NO_3)]NO_3$ (**1**) by X-ray crystallography. The crystal structure of **1** shows 1:1 metal:ligand stoichiometry and helps to understand the observed PET-Off-CHEF-On sensing mechanism. LOD values of $\mathbf{H_2L1}$ and $\mathbf{H_2L2}$ toward metal ions are found to be $\sim10^{-8}$ and $\sim10^{-7}$ M, respectively. Large Stokes shifts of the probes against analytes (∼100 nm) make them a suitable candidate for biological cell imaging studies. Robson type phenol based macrocyclic fluorescence sensors are very scarce in the literature. Therefore, the tuning of structural parameters as the number and nature of donor atoms, their relative locations and presence of rigid aromatic groups can lead to the design of new chemosensors, which can accommodate different charged/neutral guest(s) inside its cavity. The study of the spectroscopic properties of this type of macrocyclic ligands and their complexes might open a new avenue of chemosensors.

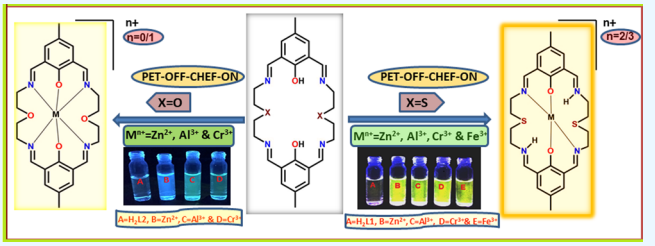

INTRODUCTION

Metals are crucial for living systems as they are actively participating in many biological processes. Among them, alkali and alkaline earth metals like Na, K, Ca, and Mg play crucial roles in osmotic regulation, biomineralization, etc., whereas transition metals like Fe, Zn, Cu, Mn, Co, Ni, Mo, and V are important for catalysis, metabolism, and signaling processes.[1,2] Typically, transition metals are present at trace levels in biological systems,[1] and they act as cofactors in diverse enzymes like cytochrome oxidase, histidine ammonia-lyase, glutamate mutase, catalase, etc.,[3,2] due to their electronic structures and redox properties. On the contrary, overdose or deficiency of transition metals are responsible for acute and long-term diseases, including heart disease, cancer and neurodegeneration.[4] Therefore, the assessment and understanding of the distribution of metal ions in living systems are fundamental for homeostasis and its related diseases.[4] Among different techniques, fluorescence spectroscopy is recognized as a useful tool to sense biologically important metal ions and, thus, widely used in biology, physiology, pharmacology, and in environmental science also. In this respect, tailored molecular chemosensors can be highly specific and sensitive toward analyte molecules with fast response time.[5] Chemosensors that can detect more than one analyte simultaneously have attracted great attention in recent years. This not only reduces production costs but also improves analysis time.[6] However, the development of fluorescence chemosensors that can both recognize multiple analytes and differentiate them still remains a great challenge.[7]

In this context, we are mainly concentrating on chemosensor which can detect Zn^{2+}, Al^{3+}, Cr^{3+} and Fe^{3+} ions.[8−16] Iron and zinc are the first and second most abundant transition metals

Received: October 11, 2022
Accepted: January 31, 2023
Published: February 13, 2023

present in human body.[17] In many biochemical processes, both iron and zinc play essential role to complete the biocycle. Iron is indispensable for oxygen storage and transport at the cellular level.[18] Whereas, zinc-containing active sites are present in many metalloenzymes such as carbonic anhydrase, carboxypeptidase A, alcohol dehydrogenase, RNA polymerase, etc.[19] However, the imbalance of both ions is responsible of different neurological disorders as Alzheimer's disease.[20] The presence of chromium decreases uptake of iron and thus reduces oxidative stress, heart disease, cancer, osteoporosis, and arthritis. The scarcity of chromium can raise the risk associated with diabetes and cardiovascular diseases.[21,22] Aluminum is one of the most used metals by our society. Its wide and multidimensional role in industry as well as in daily life provides some comfort, but excess accumulation in the human body causes several serious health issues as Alzheimer's disease, amyotrophic lateral sclerosis, encephalopathy, Parkinson's disease, etc.[23−25] Fluorometric detection of these metal ions (Al^{3+}, Zn^{2+}) has been reported by several physicochemical "Turn-On" processes like photo induced electron transfer (PET), chelation induced enhanced fluorescence (CHEF), fluorescence resonance energy transfer (FRET), intermolecular charge transfer (ICT).[26−30] On the other hand, Cr^{3+} and Fe^{3+}, due to their paramagnetic nature of, can act as fluorescence quenchers rather than as activators.[8−15]

Generally, rhodamine, anthraquinone, BODIPY, salicylaldehyde, fluorescein and coumarin based chemosensors are used for trivalent cation sensing,[31−37] while for Zn^{2+} sensing chemosensors are based typically on di-2-picolylamine (DPA),[38−41] quinoline,[42−47] bipyridyl,[43] etc. units. Therefore, simultaneous sensing of all these cations in a single platform is a challenging task. Several parameters such as avoiding multistep preparations of the probes, solubility in common solvents, high sensing ability, real sample analysis and biological applications (Chart S1, Supporting Information) need to be considered for the preparation of the chemosensors.

Nature chooses macrocyclic ligands for stability of variety of biological systems which include chlorophyll, hemoglobin and vitamin B12 etc. Macrocyclic Schiff-base ligands have wide applicability in the fields of analytical process, medicinal chemistry, supramolecular chemistry,[48a,b] biochemistry,[48c,d] organic synthesis, materials science,[48e] recognition[48f] catalysis,[48g] etc. Synthetic macrocyclic complexes are much more thermally stable, more resistance toward degradation, chemically unreactive to acids and alkali in comparison with their metal-containing open-chain analogues. Metal coordination gives structural rigidity to the macrocyclic ligand so that the system can emulate active site structure of a metalloprotein.[48h] In spite of this, it is important to mention that most of the reported chemosensors for metal ions are of acyclic nature and macrocyclic chemosensors are uncommon.[49]

Cyclodextrin, pillar[n]arene, and metal−organic coordination macrocycles are some interesting macrocyclic compounds which exhibit interesting applications in the fields of molecular sensing, self-assembly, catalysis, molecular machines etc.[50−53] Important structural parameters of Robson-type macrocyclic Schiff-bases[54] like number and nature of donor atoms, their relative locations, presence of rigid aromatic groups can be tuned to accommodate different charged or neutral guest(s) inside the cavity. Ōkawa and co-workers have made many modifications in the basic structure of phenol based macrocyclic ligands like using of different lateral chains, introduction of an additional donor atom on one lateral chain or made partial or full saturation of azomethine bond. Macrocycles with symmetrical lateral chains give hetero dinuclear Cu(II)M(II) or M(II)Cu(II) [M(II) = Mn, Co, Ni, Cu, Zn] compounds depending on the synthetic procedure and nature of donor sites.[55,56] A. E. Martell et al. have synthesized hydrogenated macrocyclic ligands to study their basicity and their coordination compounds are further studied for phosphate di ester catalytic process.[57] Some macrocyclic chemosensors are collected in Chart S2. Among them, most of the chemsonsors are selective toward single metal ion. G. Ambrosi et al. have prepared a fluorescent oxadiazole derivative which selectivity detect Zn(II) in alkaline medium. The synthesis involved multistep procedure and presence of alkaline medium restrict cell imaging study of the chemosensor.[58a] B. Ghanbari and his group have reported two naphthalene based aza-crown macrocyclic ligands for selective detection of Al(III) ions in ethanol. The LOD values for Al(III) cation by the chemosensors were found to be $\sim 10^{-9}$ M order.[58b] A piperazine linked diimine phenol has been reported by S. Goswami and his group which selectively detect Zn(II) in mixed aquous medium. The Zn-chemosensor complex has been utilized as a receptor for dihydrogen phosphate (DHP) sensing in aqueous medium by metal displacement approach resulting quenching of fluorescence intensity and generating the free chemosensor. The chemosensor further used for sensing of Zn^{2+} and DHP in living cells.[58c] Another aza-crown macrocyclic chemosensor, namely, 1-Hydroxy-diaza-15-Crown-4, was used by C. Sinha and co-workers for chromogenic sensing of Al^{3+} in DMSO-water medium. The probe also exhibits fluorescent turn on in the presence of Al^{3+} and Zn^{2+} ions. Furthermore, fluorescence cell imaging study of the probe had been performed in SCC084 (Human Oral carcinoma) cell lines.[58d] P. K. Panda and his group have designed a novel meso-expanded calix[4]pyrrolemacrocycle, where a rigid o-phenylene unit is incorporated as a spacer between the α,α'-positions of the tetrapyrrane moiety. It belongs to its smallest expanded analogue. Its selectivity detects fluoride ion via a turn-on response.[58e] R. Azadbakh et al. have developed a novel fluorescent nanochemosensor starting from a reduced macrocyclic Schiff Base ligand. It acts as a highly selective and sensitive sensor toward Fe(III) and I^- through a fluorescence "'on−off'" process, with a limit of detection in nM range.[58f] D. Das et al. have found that an acyclic phenol-based Schiff base compartmental ligand, *N*,*N*′-propylene-bis(3-formyl-5-*tert*-butylsalicylaldimine) upon reaction with Zn(II) produced a dinuclear Zn(II)-cyclic compound. The acyclic compound containing C═N bonds undergone hydrolysis in the presence of Lewis acid $ZnCl_2$ in organic-aqua medium. Free ligand exhibits yellowish green fluorescence emission at 523 nm when excited at 437 nm in 1:1 water− acetonitrile. In the presence of Zn^{2+}, a new fluorescence emission band appears at 481 nm and the intensity enhanced gradually. Thus, the acyclic compound acts as a ratiometric fluorescence chemodosimeter for the selective detection of Zn(II) ions.[58g] V. Fusi et al. have synthesized a cyclophane macrocyclic probe containing 1,3-bis(benzo[d]oxazol-2-yl)phenyl fluorophore as sensing unit. It acts as a PET-mediated fluorescent chemosensor, at acidic medium. The macrocyclic probe signals the presence of Zn(II) and Cd(II) metal ions via fluorescence enhancement in a mixed acetonitrile−aqueous medium at physiological pH. Furthermore, experimental and theoretical studies suggested the formation of both mononuclear and dinuclear Zn^{2+}-probe complexes, while only the mononuclear complex was found in

https://doi.org/10.1021/acsomega.2c06549
ACS Omega 2023, 8, 7479−7491

the case of Cd^{2+}.[58h] P. Paul and his group have designed a fluorescent compound involving a Re(I)-bipyridine moiety as a fluorogenic unit and amide-incorporated modified calix[4]-arene as recognition moiety. It behaves as a dual chemosensor which selectively enables turn-on fluorescence in the presence of Hg^{2+} and naked eye colorimetric detection of Cu^{2+} among different metal ions.[58i]

Here, we report two aza-phenol based macrocyclic Schiff base ligands, **H_2L1** [**H_2L1**=1,11-dimethyl-6,16-dithia-3,9,13,19-tetraaza-1,11(1,3)-dibenzenacycloicosaphane-2,9,12,19-tetraene-1,11-diol] and **H_2L2** as multi analyte chemosensors which fluorimetrically detects different cations (**H_2L1**: Zn^{2+}, Al^{3+}, Cr^{3+} and Fe^{3+} and **H_2L2**: Zn^{2+}, Al^{3+} and Cr^{3+}) in 1X PBS solution. The interaction of the metal ions with our chemosensors have been examined by absorption, emission and ^{1}H NMR spectroscopies as well as by elemental and ESI-MS$^+$ analysis. The binding mode of Zn^{2+} with **H_2L1** (complex **1**) has been established by X-ray crystallography. Both the chemosensors exhibit ∼6-fold enhancement of emission intensity in the presence of different metal ions. The LOD values of the probes, **H_2L1** and **H_2L2** toward these cations are found to be $\sim10^{-8}$ and $\sim10^{-7}$ M, respectively. Bioimaging studies of **H_2L1** and **H_2L2** using *HepG2* cells along with MTT assays were also performed. The use of aza-phenol based macrocyclic chemosensors for multiple-analyte detection is a unique attempt. The judicious choice of donor centers and ligand topologies results in selective coordination of selected metal ions with high binding constants. The study of the spectroscopic properties of such a type of macrocyclic ligands and of their metal complexes may open new avenues for obtaining multianalyte sensors.

RESULTS AND DISCUSSION

Synthesis and Characterization. 2,6-Diformyl-4-methyl-phenol (DFP) has been prepared following a standard procedure.[59] 2,2′-Thiobisethylamine or hydrochloride salt of 2,2′-oxybis(ethan-1-amine) was mixed with DFP in 1:1 molar ratio in a chloroform−methanolic (1:9, v/v) solution under reflux (Scheme S1, Supporting Information) to generate the Schiff base ligands **H_2L1** and **H_2L2** without further purification. **H_2L1** and **H_2L2** were thoroughly characterized using different spectroscopic methods (UV−vis, FT-IR, ^{1}H and ^{13}C NMR) and by elemental analysis. In the ESI-MS$^+$ analysis, the base peak was found at m/z = 497.18 and 465.23, corresponding to $[\mathbf{H_2L1}+H]^+$ and $[\mathbf{H_2L2}+H]^+$, respectively (Figure S1 and Figure S2, Supporting Information). In the FT-IR spectra of the chemosensors a broad band at around ∼3300 cm^{-1} indicates the presence of the phenolic−OH groups and the band at ∼1640 cm^{-1} is attributed to the C═N (for azomethine) stretching frequency (Figure S3).

H_2L1 and **H_2L2** reacts with respective metal ions (**H_2L1**: Zn^{2+}, Al^{3+}, Cr^{3+} and Fe^{3+}; **H_2L2**: Zn^{2+}, Al^{3+} and Cr^{3+}) in 1:1 ratio in methanol to produce the complexes **1**−**7**, respectively (Scheme 1). Complexes were characterized by different spectroscopic techniques, elemental and ESI-MS$^+$ analyses. In the FT-IR spectra of all seven complexes, **1**−**7** show characteristic stretching frequencies at ∼1640 cm^{-1} υ(C═N), ∼770 cm^{-1} υ(C−H) and ∼1340 cm^{-1} ($\upsilon(NO_3^-$, asymmetric stretch) (Figures S4 and S5).

Crystal Structure Description of [Zn(H_2L1)(NO_3)]NO_3 (1). We have successfully crystallized [Zn(**H_2L1**)(NO_3)]NO_3 (**1**) form slow evaporation of a methanolic solution of zinc nitrate hexahydrate and **H_2L1**. Crystals of **1** are present in

Scheme 1. Route to the Synthesis of Complexes 1−7

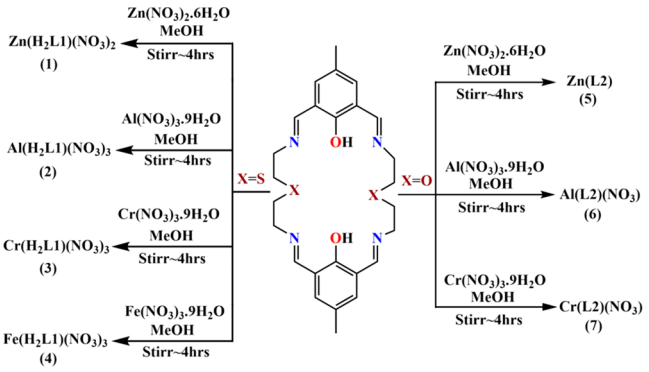

triclinic form with *P*-1 space group (Table S1, Supporting Information). The crystal structural is shown in Figure 1.

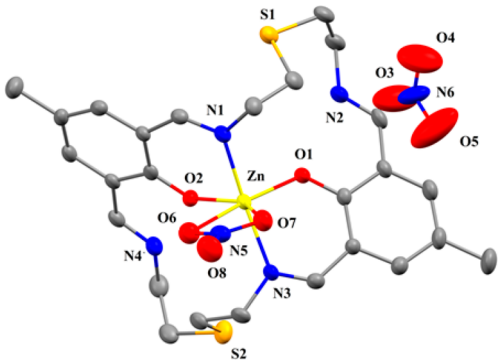

Figure 1. Crystal structure of the asymmetric unit of **1**. Atoms are shown as 30% thermal ellipsoids. H atoms are omitted for clarity.

Selected bond distances and angles are collected in Table S2. The asymmetric unit consists of the whole molecule, the Zn^{2+} bound chemosensor and two nitrate ions, one bound with the metal ion in the first coordination sphere and the other one acting as a counteranion. In **1**, the Zn^{2+} center adopts a distorted octahedral geometry in which the imine nitrogens (N1, N3) are placed in axial positions, while the phenoxido oxygen atoms (O1, O2) and one nitrate anion, coordinated in a bidentate fashion (O6, O7), occupy the equatorial plane. Interestingly, the remaining uncoordinated imine nitrogens (N1, N3) are present in protonated form. Sulfur atoms (S1, S2) also remain uncoordinated. The Zn−N_{imino} and Zn−$O_{phenoxido}$ bond distances are 2.096(4)Å (Zn−N1), 2.094(4)Å (Zn−N3), 2.025(3)Å (Zn−O1), and 2.004(3)Å (Zn−O2), respectively. The other Zn−O distances are 2.362(4) Å (Zn−O6) and 2.363(4)Å (Zn−O7), respectively. The equatorial angles vary from 54.01(12)° to 112.54(12)°. The axial N1−Zn−N3 angle is 165.64(14)°. Complex **1** is further stabilized by different supramolecular interactions including $\pi\cdots\pi$ (3.792 Å), C−H$\cdots\pi$ (3.692 Å) and chalcogen interaction (3.206 Å) to form a one-dimensional chain along the "*a*" axis (Figure S6).

Importantly, the crystal structure proves the PET-off CHEF-on fluorescence sensing. It also supports the experimentally observed m/z value of 279.96, which corresponds to the molecular ion peak of $[Zn(\mathbf{H_2L1})]^{2+}$ (Figure S7).

NMR Studies. ^{1}H and ^{13}C NMR of **H_2L1**, **H_2L2** and of complexes **1**, **2**, **5**, and **6** were recorded in DMSO-d_6 solvent. In ^{1}H NMR of **H_2L1**, the imine (H−C═N) protons give a peak at 8.48 ppm. The aromatic protons appear at 7.35 ppm,

https://doi.org/10.1021/acsomega.2c06549
ACS Omega 2023, 8, 7479−7491

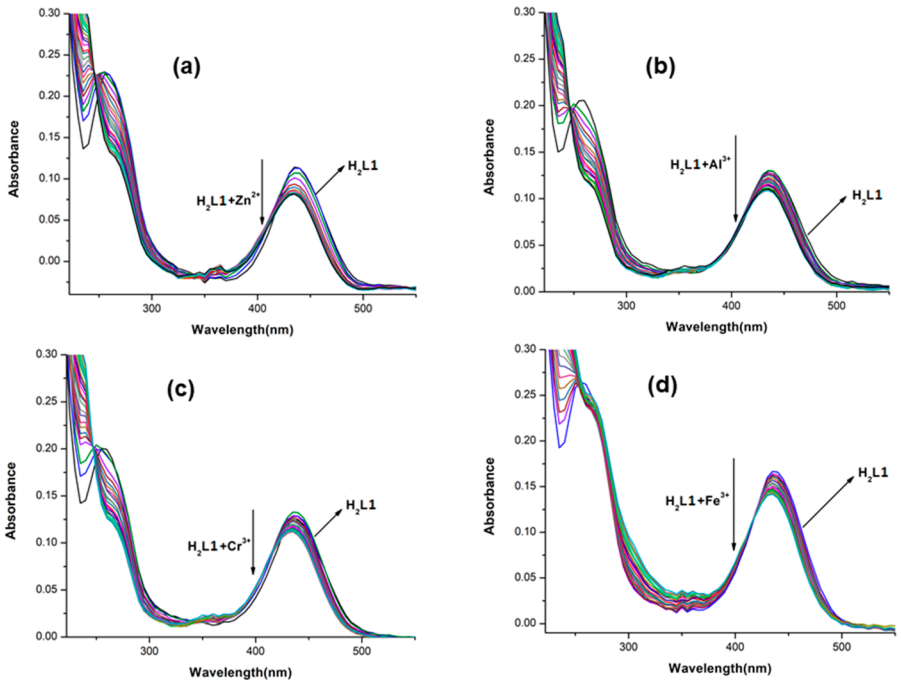

Figure 2. Absorbance titration of $\mathbf{H_2L1}$ (20 μM) with gradual addition of (a) Zn^{2+} (0−20 μM); (b) Al^{3+}(0−20 μM); (c) Cr^{3+}(0−20 μM), and (d) Fe^{3+}(0−20 μM) in 1X PBS solution.

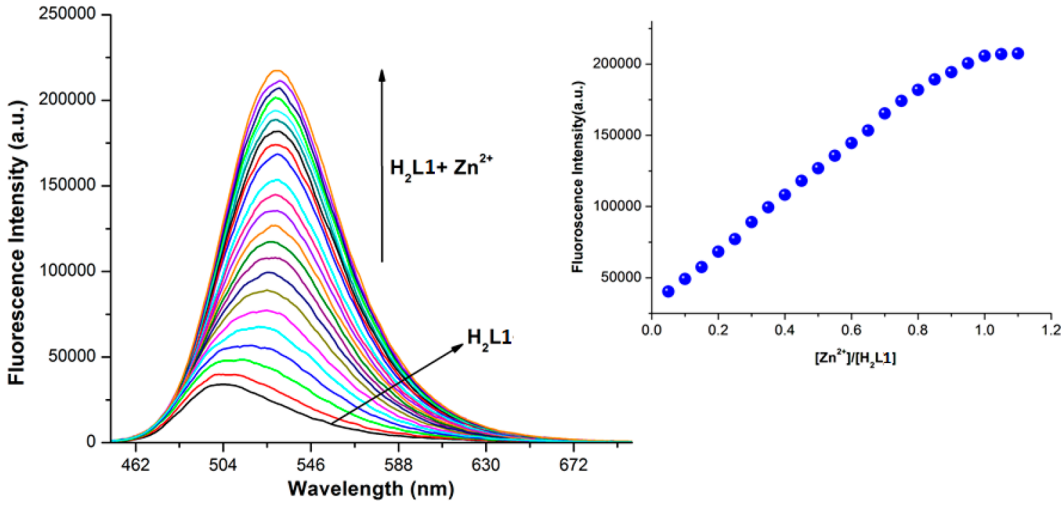

Figure 3. Fluorescence titration of $\mathbf{H_2L1}$ (20 μM) with gradual addition of Zn^{2+} (0−22 μM) in 1X PBS solution and corresponding fluorescence intensity versus molar ratio plot (λ_{exc} = 435 nm).

while the aliphatic protons appear at 3.74 and 2.87 ppm, respectively. Methyl protons are found at 2.19 ppm (Figure S8). Aromatic OH protons give a broad signal at 13.98 ppm. In the ^{13}C NMR (Figure S9) the imine carbon atoms appear at 167.10 and 161.94 ppm whereas aromatic carbon atoms appear in the range 139.93−119.42 ppm. Aliphatic carbon atoms appear in the range 55.61−32.38 ppm and methyl carbon atoms appear at 20.34 and 20.06 ppm. Similar type of ^{1}H and ^{13}C NMR spectral pattern were found for $\mathbf{H_2L2}$ also (Figures S10 and S11)

Interaction of Zn^{2+} and Al^{3+} with $\mathbf{H_2L1}$ is well explained with the help of NMR spectroscopy. In the ^{1}H NMR of **1** (Figure S12), the disappearance of phenolic −OH peaks prove the binding of the phenoxido oxygens to Zn^{2+}. The signal of the imine protons splits into two signals at 8.68 and 8.40 ppm, indicating coordinated and uncoordinated imine nitrogens. Aromatic protons appear downfield at 7.78 and 7.53 ppm. In the ^{13}C NMR spectrum of **1** (Figure S13), the signals of the imine carbons appear at 170.94 and 169.96 ppm, while the aromatic carbon atoms appear in the range of 147.62−116.55 ppm. Aliphatic carbon atoms are observed in the range of 60.50−30.62 ppm.

In the ^{1}H NMR of **2** (Figure S14), the disappearances of the phenolic −OH peaks support the binding of the phenoxido oxygens to Al^{3+}. The imine protons appear downfield shifted at 8.76 and 8.61 ppm. Both aromatic and aliphatic protons are also undergoing broadening and appear at 7.86, 7.70, 3.95, and 3.00 ppm, respectively. In the ^{13}C NMR spectrum of **2** (Figure S15), imine and aromatic carbons appear in the ranges 168.98−167.12 ppm and 146.40−117.30 ppm, respectively. Aliphatic carbon atoms are shown in the range 52.00−28.14

https://doi.org/10.1021/acsomega.2c06549
ACS Omega 2023, 8, 7479−7491

ppm. ^{1}H and ^{13}C NMR spectral data of complexes **5** and **6** are collected in Experimental Section (Figures S16−S19).

We have also performed ^{1}H NMR titration experiments of H_2**L1** and H_2**L2** with Zn^{2+} or Al^{3+} in DMSO-d_6 solvent (Figures S20−S23). Upon gradual addition of (0 to 1 equiv) metal ions to one equivalent of chemosensor, disappearance of phenolic −OH protons, significant splitting and downfield shift of imine protons, broadening and splitting of aromatic and aliphatic protons prove strong interaction between chemosensor and corresponding metal ions. The X-ray crystallographic data of complex **1** agrees with the ^{1}H NMR titration data.

Absorption Spectral Studies. The UV−vis absorption spectrum of both H_2**L1** and H_2**L2** were studied in 1X PBS solution (pH 7.4). The same buffer medium was chosen for both spectroscopic studies and biological work in order to avoid experimental errors. Characteristic bands around 435 and 265 nm suggest n → π^* and π →π^* type of transitions within the probes. The gradual addition of a Zn^{2+} (0−20 μM) solution to a 20 μM H_2**L1** solution results in a decrease in the intensity of the peak at 435 nm and a concomitant increase in absorbance at around 265 nm (Figure 2). Both the signals at 435 nm and at 265 nm do not further change after the addition of one equivalent of Zn^{2+}, suggesting 1:1 binding stoichiometry. A similar situation was observed for the trivalent cations, Al^{3+}, Cr^{3+} and Fe^{3+} (Figure 2). In the case of chemosensor H_2**L2**, upon gradual addition of metal ion (Zn^{2+}, Al^{3+} and Cr^{3+}; 0−20 μM), there is an enhancement of intensity at 440 nm (Figure S24).

Fluorescence Properties. The fluorescence spectra were recorded in 1X PBS solution at ambient conditions. Upon excitation at 435 nm, H_2**L1** exhibits weak fluorescence at 505 nm, probably due to a PET (Photo Induced Electron Transfer) process. Photoinduced intramolecular electron transfer (PET) from the HOMO of the donor imine nitrogen atoms to the excited fluorophoric moiety results in excited state quenching. Addition of Zn^{2+} (0−22 μM, excitation wavelength 435 nm) to a 20 μM solution of H_2**L1** produces a gradual increase of the emission intensity and a red shift of the peak at 530 nm (Figure 3), which reaches 6-fold enhancement and a plateau for a ∼1:1 [Zn^{2+}]/ [H_2**L1**] molar ratio (Figure 3). The 1:1 binding stoichiometry has been confirmed by Job's plot analysis (Figure S25). Coordination of Zn^{2+} to H_2**L1**, increases the rigidity of the molecule via restriction of free rotation of H_2**L1** around the H−C═N bond. Moreover the PET process could not continue further due to donation of the lone pair of electrons by the imine nitrogen. Both these effects are jointly responsible for the fluorescence enhancement (CHEF effect). The apparent binding constant for the 1:1 Zn^{2+}/H_2**L1** complex was calculated using the Benesi− Hildebrand equation:[60a]

$$\{(F_{max} - F_0)/(F_x - F_0)\} = \{1 + (1/K)(1/[Zn^{2+}])\} \quad (1)$$

where K represents the metal to chemosensor binding constant. F_{max}, F_0, and F_x are fluorescence intensities in the presence of maximum [Zn^{2+}] (1 equiv for 1:1 Zn^{2+}: H_2**L1**), free ligand [H_2**L1**] (1 equiv) and any intermediate Zn^{2+} concentration (0−1.0 equiv), respectively. The binding constant (K) was estimated to be ∼1.67 × 10^5 M^{-1} (Figure S26, Table S3). The stability constant calculated with the program HypSpec ((1.22 ± 0.01) × 10^5 M^{-1}) which permits the use of multiple wavelengths to make the fitting, is in good agreement with the value obtained.[60b,c]

Similarly, addition of the trivalent metal ions Al^{3+}, Cr^{3+} and Fe^{3+} leads to a red-shift of the H_2**L1** band at 505 nm that now appears at 530 nm and to a remarkable ca. 6-fold enhancement of the emission (Figures S27−S29). A plateau of the emission is reached in all cases for 1:1 [M^{3+}]:[H_2**L1**] molar ratio. The 1:1 M^{3+}: H_2**L1** binding stoichiometry of these trivalent metal ions toward the chemo sensing probe H_2**L1** was further confirmed by Job's plot analysis (Figure S25). The selective response toward Zn^{2+}, Al^{3+}, Cr^{3+} and Fe^{3+} can be ascribed based on the Pearson principle which allows them to better fit into the macrocyclic coordination framework and coordinate with imine nitrogens and phenoxido oxygens. Again, paramagnetic metal ions like Cr^{3+} or Fe^{3+} are well-known fluorescence quenchers.[61a,b] Here, electron or energy transfer between the metal ions and fluorophores causes very fast and efficient nonradiative decay of the excited states resulting quenching of the fluorescence. An example of fluorescence enhancement in the presence of paramagnetic centers via chelation enhanced fluorescence (CHEF) mechanism is uncommon. Design of chemosensor with suitable multi dentate chelating units, which can effectively coordinate to the metal center resulting CHEF effect depends on the selection of ionophore.[61c−e] Turn-on fluorescent sensors for Cr^{3+} or Fe^{3+} ions are less reported due to the lack of selective ionophores.[61f−h] In presesence of chemosensor H_2**L1** and H_2**L2**, Cr^{3+} (both H_2**L1** and H_2**L2**) and Fe^{3+} (only H_2**L1**) form stable complexes resulting enhancement of the rigidity of the complex. The 6-fold fluorescence enhancement at 530 nm is a result of chelation-enhanced fluorescence (CHEF).[61i] Further, H_2**L1** and H_2**L2** are Schiff base ligands where C═N bond undergoes isomerization in the excited state resulting weak fluorescence. Coordination of metal ions with imine nitrogen inhibits C═N isomerization and decreased nonradiative decay of the excited-state, leading to fluorescence enhancement. In the present work, we observed an obvious enhancement of fluorescence intensity in the presence of Zn^{2+} and Al^{3+} as well as paramagnetic metal ions Cr^{3+} and Fe^{3+}. Therefore, there is a competition between the fluorescence enhancement due to the inhibition of C═N isomerization and quenching of fluorescence from the metal ion-induced electron or energy transfer processes. Our results shows that the C═N isomerization plays a predominant role.[61j−l]

Interestingly, other metal ions fail to exhibit fluorescence enhancement probably due to several reasons such as the suitable coordination geometry, conformation of the Schiff base sensor, the appropriate ion radius and sufficient binding energy, leading to selective recognition of Zn^{2+}, Al^{3+}, Cr^{3+} and Fe^{3+}. The apparent binding constants for trivalent metal bound chemosensor H_2**L1** complexes were calculated using the Benesi−Hildebrand equation.[60a] The apparent binding constant (K) values for Al^{3+}, Cr^{3+} and Fe^{3+} were estimated to be 1.82 × 10^5 M^{-1}, 1.66 × 10^5 M^{-1} and 1.26 × 10^5 M^{-1}, respectively (Figures S30−S32, Table S3).

Selectivity of H_2**L1** toward Zn^{2+}, Al^{3+}, Cr^{3+} and Fe^{3+} over other common competitive species was examined by fluorescence titration experiments in the presence of different alkali metals (Na^+ and K^+), alkaline-earth metals (Mg^{2+} and Ca^{2+}) and various transition-metal ions (Mn^{2+}, Fe^{2+}, Co^{2+}, Ni^{2+}, Cu^+, Cd^{2+} and Hg^{2+}) (Figure 4). Upon addition of different common anions like $S_2O_3^{2-}$, S^{2-}, SO_3^{2-}, HSO_4^-, SO_4^{2-}, SCN^-, N_3^-, OCN^-, AsO_4^{3-}, PO_4^{3-}, ClO_4^-, AcO^-, Cl^-, NO_3^-, $P_2O_7^{4-}$ (PPi), PF_6^-, F^- and some important bio molecules such as L-Histidine, L-Cysteine, ATP, Glutathione

https://doi.org/10.1021/acsomega.2c06549
ACS Omega 2023, 8, 7479−7491

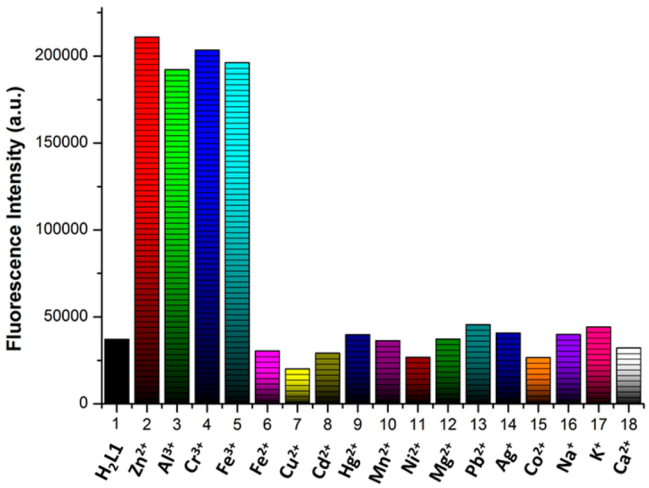

Figure 4. Relative fluorescence intensity profile of $\mathbf{H_2L1}$ in the presence of different cations (1 equiv) in 1X PBS solution [Here, 1 = only $\mathbf{H_2L1}$ (20 μM) and (2−18) = $\mathbf{H_2L1}$ (20 μM) + M^{n+} (20 μM)].

(Figure S33) in 1X PBS solution to the chemosensor no significant fluorescence enhancement was noticed.

The competition assay experiments were performed either individually for Zn^{2+} (1.0 equiv) and trivalent metal ions (Al^{3+}, Cr^{3+} and Fe^{3+}) (1.0 equiv) or in the presence of other metal ions (5.0 equiv) and common anions in 5-fold excess (5.0 equiv) in the same solvent system. Experimental results show that negligible enhancement or quenching occurs either in the presence of common cations (Figure 5, S34−S36) or common anions and some important bio molecules (Figures S37−S40).

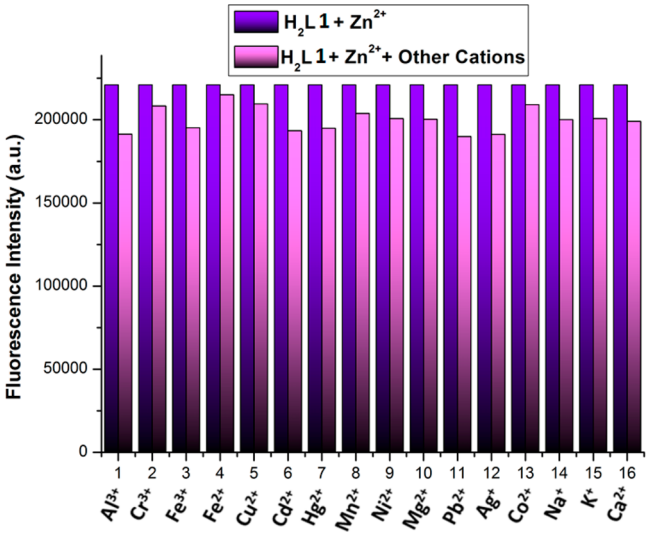

Figure 5. Relative fluorescence intensity profile of [$\mathbf{H_2L1}$+Zn^{2+}] system in the presence of different cations in 1X PBS solution [Here, $\mathbf{H_2L1}$ (20 μM); Zn^{2+} (20 μM); other cations (100 μM)].

$\mathbf{H_2L1}$ shows a distinct color change under UV light in the presence of Zn^{2+} and trivalent cations (Al^{3+}, Cr^{3+} and Fe^{3+}) in 1X PBS solution. $\mathbf{H_2L1}$ shows greenish-yellow fluorescence in the presence of Zn^{2+} and trivalent cations (Al^{3+}, Cr^{3+} and Fe^{3+}) (Figure 6).

Reversibility and regeneration of the free chemosensor are two important aspects for real time applications. In this experiment, the sodium salt of ethylenediaminetetraacetic acid

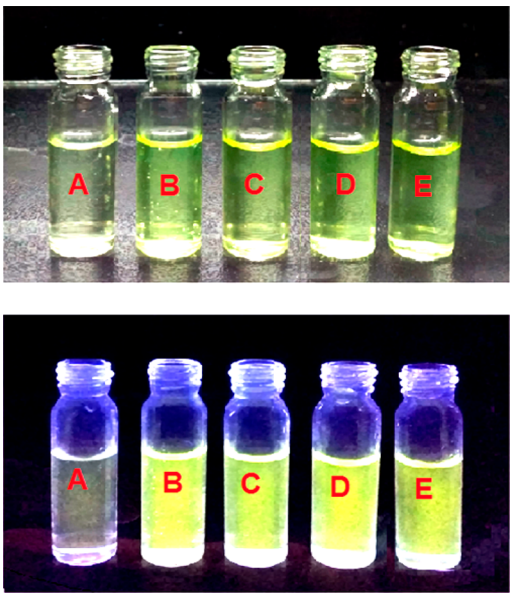

Figure 6. Visual color changes of chemo sensors ($\mathbf{H_2L1}$) in the presence of Zn^{2+}, Al^{3+}, Cr^{3+} and Fe^{3+} ions in 1X PBS solution. Here, A = $\mathbf{H_2L1}$ (20 μM), B= $\mathbf{H_2L1}$ (20 μM) + Zn^{2+} (20 μM), C-E = $\mathbf{H_2L1}$ (20 μM) + M^{3+} (M = Al, Cr and Fe) (20 μM), respectively. The upper images were taken under normal light, and the lower images were taken under UV lamp.

(Na_2EDTA) is used as strong chelating ligand. After the addition of 1 equiv of Na_2EDTA to a solution of Zn^{2+} and $\mathbf{H_2L1}$, the fluorescence changes from greenish-yellow to colorless with obvious decrease in fluorescence intensity, confirming the regeneration of the free probe. Similarly, in the presence of either Al^{3+} or Cr^{3+} or Fe^{3+} and $\mathbf{H_2L1}$, addition of 1 equiv of Na_2EDTA results in a change of the fluorescence from greenish-yellow to colorless indicating again regeneration of the free probe (Figure S41).

The limit of detection (LOD) is an important parameter of chemosensor $\mathbf{H_2L1}$ for real sample analysis. LOD of the chemosensor toward Zn^{2+}, Al^{3+}, Cr^{3+} and Fe^{3+} were calculated using the 3σ method.[62] The LODs for the Zn^{2+}, Al^{3+}, Cr^{3+} and Fe^{3+} are 7.99×10^{-8} M, 9.65×10^{-8} M, 8.86×10^{-8} M and 8.43×10^{-8} M, respectively, indicating that these metal ions could be detected quantitatively.

Interestingly, chemosensor $\mathbf{H_2L2}$ exhibits similar type of fluorescence properties toward Zn^{2+}, Al^{3+} and Cr^{3+} ions. Free chemosensor exhibits weak fluorescence at 540 nm upon excitation at 440 nm. Addition of different metal ions (Zn^{2+}, Al^{3+} and Cr^{3+}) results in 6-fold enhancement of fluorescence intensity at 530 nm (Figures S42−S44). The 1:1 M^{2+}/ M^{3+}: $\mathbf{H_2L2}$ binding stoichiometry was also confirmed by Job's plot analysis (Figure S45). All the relevant results are collected in the Supporting Information (Figures S46−S54). The apparent binding constant (K) values and LOD values toward Zn^{2+}, Al^{3+} and Cr^{3+} were estimated to be 1.27×10^5 M^{-1}, 1.59×10^5 M^{-1} and 1.53×10^5 M^{-1}, respectively and 10^{-7} M range (Figures S55−57,Table S3).

Lifetime and Quantum Yield Measurements. Lifetime experiment of $\mathbf{H_2L1}$, $\mathbf{H_2L2}$ and complexes **1**−**7** were performed at 298 K in 1X PBS solution. The average fluorescence decay lifetimes of all the compounds were determined by using the formula $\tau_f = a_1\tau_1 + a_2\tau_2$, where a_1 and a_2 are relative amplitude of decay process. The average

https://doi.org/10.1021/acsomega.2c06549
ACS Omega 2023, 8, 7479−7491

fluorescence lifetime of H_2L1, H_2L2 and complexes **1**−**7** are 0.39, 4.58 and 1.30, 1.06, 1.18, 1.47, 4.75, 4.72, and 4.73 ns, respectively (Figure 7, Figure S58 and Table S4)

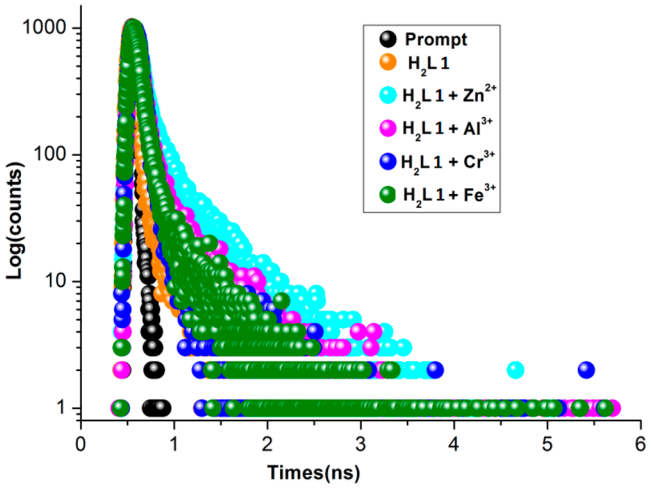

Figure 7. Time-resolved fluorescence decay curve (logarithm of normalized intensity vs time in ns) of H_2L1 and H_2L1+M^{n+} (M^{n+} = Zn^{2+}, Al^{3+}, Cr^{3+} and Fe^{3+}), respectively.

Fluorescence quantum yields (Φ) of free H_2L1, H_2L2 and complexes **1**−**7** were calculated using the following formula:

$$\Phi_{sample} = \{(OD_{standard} \times A_{sample} \times \eta^2_{sample}) / (OD_{sample} \times A_{standard} \times \eta^2_{sample})\} \times \Phi_{standard}$$

where A is the area under the emission spectral curve, OD is the optical density of the compound at the excitation wavelength and η is the refractive index of the solvent. Here the value of $\Phi_{standard}$ is taken as 0.52 (for Quinine Sulfate). The values of Φ for H_2L1, H_2L2 and complexes **1**−**7** are found to be 0.04, 0.13 and 0.15, 0.19, 0.13, 0.12, 0.27, 0.25, and 0.23 respectively (Table S4).

Cell Imaging Study. A fluorescence microscopic study was performed to envisage the cellular uptake of both ligands (H_2L1 and H_2L2) (10 μM), Zn^{2+} salt (10 μM), Al^{3+} salt (10 μM),Cr^{3+} salt (10 μM) and Fe^{3+} salt (10 μM), in *HepG2* cells. A moderate green signal is observed in the case of the cells treated with the ligand. The intensity of the green signal gets enhanced significantly when the cells were treated with H_2L1 or H_2L2 and respective metal salts. No fluorescence was observed in case of the untreated cells. Thus, we can conclude that the cells readily uptake H_2L1 and H_2L2 as well as its Zn^{2+}, Al^{3+}, Cr^{3+} and Fe^{3+}complexes, which results in prominent green fluorescent signals (Figure 8 and Figure S59).

Cell Survivability Assay. The in vitro cytotoxicity of the ligands was estimated for checking the biocompatibility on *WI-38* cell lines. The cells were treated with five different concentrations (20, 40, 60, 80, and 100 μg/mL) of ligand for 24 h and followed by MTT assay. It was observed that both the ligands exhibited no significant toxicities even at the highest concentration of 100 μg/mL (Figure 9 and Figure S60). Therefore, the ligands are biocompatible and highly conducive for biological applications.

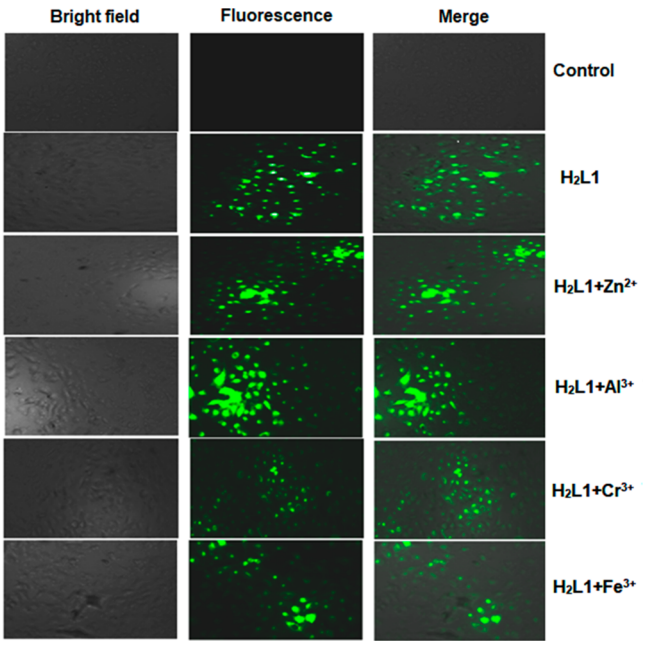

Figure 8. Bright field, fluorescence and merged microscopic images of untreated *HepG2* (Control), cells treated with H_2L1(10 μM), H_2L1(10 μM)+ Zn^{2+}(10 μM), H_2L1(10 μM) + Al^{3+}(10 μM), H_2L1 (10 μM) + Cr^{3+}(10 μM) and H_2L1 (10 μM) + Fe^{3+} (10 μM).

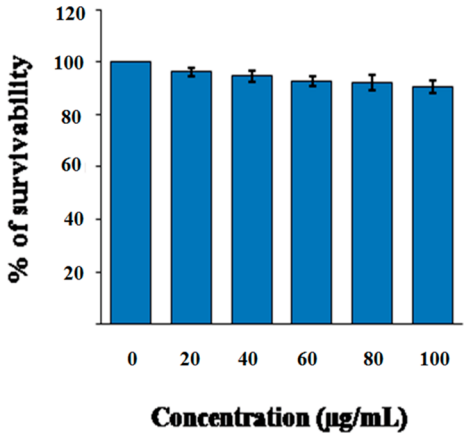

Figure 9. Cell survivability of WI-38 cells exposed to the ligand H_2L1.

SUMMARY

In this work, we have successfully developed two aza-phenol based macrocyclic fluorescence probes, H_2L1 and H_2L2 as a "turn-on" fluorescence receptor toward multiple metal ions (H_2L1 for Zn^{2+}, Al^{3+}, $Cr^{3+}$and Fe^{3+}ions; H_2L2 for Zn^{2+}, Al^{3+} and Cr^{3+} ions). Fluorescence enhancement originates from a CHEF effect owing to the coordination of metal ions with the macrocyclic ligand through the imine nitrogens and phenoxido oxygens. In presence of above metal ions around 6-fold enhancement of emission intensity in 1X PBS solution is observed.1:1 chemosensor: metal binding stoichiometry both in solid and solution phase has been proven by different techniques viz. X-ray crystallography, ESI-Mass analysis and fluorescence spectroscopy. Important parameters like reversibility and regeneration of the chemosensors have been examined in the presence of Na_2EDTA. The large Stoke shifts of the chemosensors in the presence of metal ions (∼100 nm) and low LOD values make them suitable for bioimaging

https://doi.org/10.1021/acsomega.2c06549
ACS Omega 2023, 8, 7479−7491

studies. Indeed, we have successfully performed bioimaging studies of the chemosensors using *HepG2* cells along with MTT assay. Therefore, phenol based macrocyclic probes able to behave as multianalyte detectors constitute a unique class of chemosensors. Moreover, the tuning of the macrocyclic framework and donor sites can lead to chemosensors able to accommodate different analytes with varying stoichiometries.

EXPERIMENTAL SECTION

Materials and Physical Measurements. All reagent or analytical grade chemicals and solvents were purchased from commercial sources and used without further purification. Elemental C, H, and N analysis was carried out using a Perkin−Elmer 240C elemental analyzer. Infrared spectra (400−4000 cm^{-1}) were recorded from KBr pellets on a Nicolet Magna IR 750 series-II FTIR spectrophotometer. Absorption spectra were measured with a sensitive UV−vis spectrophotometer (UV-2450 spectrophotometer (Shimadzu, Japan)) equipped with double beam light source with a 1 cm-path-length quartz cell. Electron spray ionization mass (ESI-MS^+) spectra were recorded on a MICROMASS Q-TOF spectrometer. Emission spectra were collected using a Fluoromax-4 spectrofluorometer at room temperature (298 K) under degassed condition. Fluorescence lifetimes were measured using a time-resolved spectrofluorometer from IBH, UK. Measurements of ^1H and ^{13}C NMR spectra were conducted using a BRUKER 300 spectrometer.

X-ray Crystallography. Single crystal X-ray data of **1**was collected on a Bruker SMART APEX-II CCD diffractometer using graphite monochromated MoKα radiation (λ = 0.71073 Å) at room temperature. Data processing, structure solution, and refinement were performed using the Bruker Apex-II suite program. All available reflections in $2\theta_{max}$ range were harvested and corrected for Lorentz and polarization factors with Bruker SAINT plus.[63] Reflections were then corrected for absorption, interframe scaling, and other systematic errors with SADABS.[64] The structures were solved by direct methods and refined by means of full matrix least-squares technique based on F^2 with SHELX-2018/3 software package.[65] All the non hydrogen atoms were refined with anisotropic thermal parameters. C−H hydrogen atoms were inserted at geometrical positions with U_{iso} = 1/2U_{eq} to those they are attached. Crystal data and details of data collection and refinement for complex **1** are summarized in Table S1.

Synthesis of 2,6-Diformyl-4-methylphenol (DFP). 2,6-Diformyl-4-methylphenol (DFP) was prepared following a standard literature procedure.[59]

Synthesis of Chemosensor ***H_2L1*** *[****H_2L1*** *= 1,11-Dimethyl-6,16-dithia-3,9,13,19-tetraaza-1,11(1,3)-dibenzenacycloicosaphane-2,9,12,19-tetraene-1,11-diol].* A mixture of 2,6-diformyl-4-methylphenol (2.0 mmol, 0.3283 g) and 2,2-thiobis(ethylamine) (2.0 mmol, 0.2404 g) was stirred (∼30 min.) and then heated to reflux for 4 h in a chloroform−methanol (1:9 v/v) mixture. An orange colored gummy mass was obtained after evaporation of the solvent.

Yield: 0.427g (86%). Anal. Calc. for $C_{26}H_{32}N_4O_2S_2$: C 60.40%; H 6.26%; N 9.99%. Found: C 60.19%; H 6.17%; N 10.02%. IR (cm^{-1}, KBr): υ(C═N) 1634s; ν(O−H) 3363s. ESI-MS^+ in MeOH: The base peak was detected at m/z = 497.18, corresponding to $[\mathbf{H_2L1}+H]^+$. UV−vis, λ_{max} (nm), (ε (dm^3 $mol^{-1}cm^{-1}$)) in 1X PBS solution: 435 (6450), 265(5850).

^1H NMR (DMSO-d_6, 300 MHz) δ ppm: 2.19 (Ar−CH_3) (s, 6H), 2.87 (−CH_2) (t, 8H, J_1= J_2 = 6 Hz), 3.74 (−CH_2) (t, 8H, J_1 = J_2 = 6 Hz), 7. 35 (Ar−H) (s, 4H), 8.48 (−CH═N) (s, 4H), 13.98(Ar−OH) (s, 2H).

^{13}C NMR (DMSO-d_6, 75 MHz) δ ppm: 20.06, 20.34, 32.38, 33.49, 52.89, 55.61, 119.42,121.08, 124.77, 125.49, 126.62, 132.83, 135.14, 139.93, 161.94,167.10.

Synthesis of Chemosensor ***H_2L2*** *[****H_2L2*** *=1,11-Dimethyl-6,16-dioxa-3,9,13,19-tetraaza-1,11(1,3)-dibenzenacycloicosaphane-2,9,12,19-tetraene-1,11-diol].* A mixture of hydrochloride salt of 2,2′-oxybis(ethan-1-amine) (2.0 mmol, 0.354 g) and sodium acetate (6.0 mmol, 0.492 g) was stirred for ∼30 min in methanol solvent. A clear solution was found. After that 2,6-diformyl-4-methylphenol (2.0 mmol, 0.328 g) was added to this solution and heated to reflux for 4 h in a chloroform−methanol (1:9 v/v) mixture. Deep yellow colored solid mass was obtained after evaporation of the solvent.

Yield: 0.394g (85%). Anal. Calc. for $C_{26}H_{32}N_4O_4$: C 67.22%; H 6.94%; N 12.06%. Found: C 67.19%; H 6.91%; N 12.02%. IR (cm^{-1}, KBr): υ(C═N) 1637s; ν(O−H) 3392. ESI-MS^+ in MeOH: The base peak was detected at m/z = 465.23, corresponding to $[\mathbf{H_2L2}+H]^+$. UV−vis, λ_{max} (nm), (ε (dm^3 $mol^{-1}cm^{-1}$)) in 1X PBS solution: 440 (2975), 348(2350).

^1H NMR (DMSO-d_6, 300 MHz) δ ppm: 2.13 (Ar−CH_3) (s, 6H), 3.55(−CH_2) (s, 8H) 3.67 (−CH_2) (t, 8H, J_1 = J_2 = 3 Hz), 7.21 (Ar−H) (s, 4H), 8.36 (−CH═N) (s, 4H), 13.82(Ar−OH) (s, 2H).

^{13}C NMR (DMSO-d_6, 75 MHz) δ ppm: 20.36, 20.44, 58.89, 59.35, 59.16, 69.89, 121.12, 126.20, 126.47, 132.10, 154.42, 159.48, 160.13, 162.40, 164.00, 170.50.

Synthesis of Complex (1) {$[Zn(H_2L1)(NO_3)]NO_3$}. A 5 mL methanolic solution of zinc nitrate hexahydrate (1.0 mmol, 0.297 g) was added dropwise to a 20 mL methanolic solution of $\mathbf{H_2L1}$ (1.0 mmol, 0.497 g). The resultant reaction mixture was stirred for ∼4 h. Yellow colored block shape crystals were obtained after few days.

Yield: 0.514g (75%). Anal. Calc. for $C_{26}H_{32}N_6O_8S_2Zn$: C 45.52%; H 4.70%; N 12.25%. Found: C 45.44%; H 4.62%; N 12.19%. IR (cm^{-1}, KBr): υ(C═N) 1638s; υ(NO_3^-)1363s; ν(C−H) 769 s. ESI-MS^+ in MeOH: The base peak was detected at m/z = 279.96, corresponding to $[Zn(\mathbf{H_2L1})]^{2+}$. UV−vis, λ_{max} (nm), (ε (dm^3 $mol^{-1}cm^{-1}$)) in 1X PBS solution: 435(3900), 255(11500).

^1H NMR (DMSO-d_6, 300 MHz) δ ppm: 2.31 (−CH_3) (s, 6H), 3.01 (s, 2H), 3.07 (s, 2H), 3.71 (s, 2H), 3.93 (−CH_2) (s, 2H), 7.53 (Ar−H) (s, 2H), 7.78 (Ar−H) (s, 2H,), 8.40 (−CH═N) (s, 2H), 8.68 (−CH═N) (s, 2H,).

^{13}C NMR (DMSO-d_6, 300 MHz) δ ppm: 19.63, 19.84, 30.62, 34.50, 55.05, 60.50, 116.55, 121.20, 122.38, 123.78, 125.49, 141.18, 141.82, 147.62, 169.96, 170.94.

Synthesis of Complex (2) {$[Al(H_2L1)(NO_3)](NO_3)_2$}. A 5 mL methanolic solution of aluminum nitrate nonahydrate (1.0 mmol, 0.375 g) was added dropwise to a 20 mL methanolic solution of $\mathbf{H_2L1}$ (1.0 mmol, 0.497 g). The resultant reaction mixture was stirred for ∼4 h. A greenish-yellow solid mass was obtained after evaporation of the solvent.

Yield: 0.517 g (73%). Anal. Calc. for $C_{26}H_{32}N_7O_{11}S_2Al$: C 44.00%; H 4.55%; N 13.82%. Found: C 43.98%; H 4.50%; N 13.76%. IR (cm^{-1}, KBr): υ(C═N) 1638s; υ(NO_3^-)1339s; ν(C−H) 772 s. ESI-MS^+ in MeOH: The base peak was detected at m/z = 174.85, corresponding to $[Al(\mathbf{H_2L1})]^{3+}$ (Figure S61). UV−vis, λ_{max} (nm), (ε (dm^3 $mol^{-1}cm^{-1}$)) in 1X PBS solution: 435 (5350), 255 (10300).

https://doi.org/10.1021/acsomega.2c06549
ACS Omega 2023, 8, 7479−7491

^{1}H NMR (DMSO-d_6, 300 MHz) δ ppm: 2.26 ppm (−CH_3) (s, 6H), 3.00 (s, 4H), 3.95 (−CH_2) (s, 4H), 7.70 (Ar−H) (d, 2H, J = 9 Hz), 7.86 (Ar−H) (s, 2H), 8.61 (−CH═N) (d, 2H, J = 12 Hz), 8.76 (−CH═N) (s, 2H).

^{13}C NMR (DMSO-d_6, 300 MHz) δ ppm: 20.00, 20.07, 28.14, 28.64, 30.35, 30.94, 31.72, 32.12, 50.75, 52.00, 117.30, 117.38, 119.44, 123.06, 123.74, 124.73, 125.73, 129.76, 132.87, 137.84,139.89, 146.40, 167.12, 167.17, 168.81, 168.98.

Synthesis of Complex (3) {[Cr(H_2L1)(NO_3)](NO_3)$_2$}. A 5 mL methanolic solution of chromium nitrate nonahydrate (1.0 mmol, 0.400 g) was added dropwise to a 20 mL methanolic solution of **H_2L1** (1.0 mmol, 0.497 g).The resultant reaction mixture was stirred for ∼4 h. A wine red colored solid mass was obtained after evaporation of the solvent.

Yield: 0.543g (74%). Anal. Calc. for $C_{26}H_{32}N_7O_{11}S_2Cr$: C 42.51%; H 4.39%; N 13.35%. Found: C 42.49%; H 4.35%; N 13.30%. IR (cm^{-1}, KBr): υ(C═N) 1634s; υ(NO_3^-)1305s; ν(C−H) 818s.UV−vis, λ_{max} (nm), (ε (dm^3 mol^{-1}cm^{-1})) in 1X PBS solution: 435 (5495), 255 (10000).

Synthesis of Complex (4) {[Fe(H_2L1)(NO_3)](NO_3)$_2$}. A 5 mL methanolic solution of iron nitrate nonahydrate (1.0 mmol, 0.404 g) was added dropwise to a 20 mL methanolic solution of **H_2L1** (1.0 mmol, 0.497 g). The resultant reaction mixture was stirred for ∼4 h. A dark brown colored solid mass was obtained after evaporation of the solvent.

Yield: 0.568g (77%). Anal. Calc. for $C_{26}H_{32}N_7O_{11}S_2Fe$: C 42.28%; H 4.37%; N 13.28%. Found: C 42.24%; H 4.32%; N 13.19%. IR (cm^{-1}, KBr): υ(C═N) 1632s; υ(NO_3^-)1332s; ν(C−H) 762s.UV−vis, λ_{max} (nm), (ε (dm^3 mol^{-1}cm^{-1})) in 1X PBS solution: 435 (7000), 260 (12450).

Synthesis of Complex (5) [Zn(L2)]. A 5 mL methanolic solution of zinc nitrate hexahydrate (1.0 mmol, 0.297 g) was added dropwise to a 20 mL methanolic solution of **H_2L2** (1.0 mmol, 0.464 g). The resultant reaction mixture was stirred for ∼4 h. Yellow colored solid mass was obtained after evaporation of the solvent.

Yield: 0.410g (78%). Anal. Calc. for $C_{26}H_{30}N_4O_4Zn$: C 59.15%; H 5.73%; N 10.61%. Found: C 59.10%; H 5.69%; N 10.58%. IR (cm^{-1}, KBr): υ(C═N) 1661s. ESI-MS$^+$ in MeOH: The base peak was detected at m/z = 527.13, corresponding to [Zn(**L2**)+H]$^+$(Figure S62). UV−vis, λ_{max} (nm), (ε (dm^3 mol^{-1}cm^{-1})) in 1X PBS solution: 435(6850), 348(3900).

^{1}H NMR (DMSO-d_6, 300 MHz) δ ppm: 2.12 (−CH_3) (s, 6H), 3.77 (−CH_2) (t, 8H, J_1 = 6 Hz & J_2 = 3 Hz), 3.84 (s, 8H), 7.42 (Ar−H) (s, 4H), 8.54 (−CH═N) (s, 4H).

^{13}C NMR (DMSO-d_6, 300 MHz) δ ppm: 19.81, 20.10, 46.23, 48.10, 73.10, 73.69, 121.38, 124.09, 126.31, 136.52, 141.09, 141.37, 148.89, 155.79, 165.52, 172.80.

Synthesis of Complex (6) {[Al(L2)](NO_3)}. A 5 mL methanolic solution of aluminum nitrate nonahydrate (1.0 mmol, 0.375 g) was added dropwise to a 20 mL methanolic solution of **H_2L2** (1.0 mmol, 0.464 g). The resultant reaction mixture was stirred for ∼4 h. An orange colored solid mass was obtained after evaporation of the solvent.

Yield: 0.372 g (76%). Anal. Calc. for $C_{26}H_{30}N_5O_7Al$: C 56.62%; H 5.48%; N 12.70%. Found: C 56.58%; H 5.46%; N 12.65%. IR (cm^{-1}, KBr): υ(C═N) 1637s; υ(NO_3^-)1328s. ESI-MS$^+$ in MeOH: The base peak was detected at m/z = 539.50, corresponding to [Al(**L2**)(**H_2O**) (**CH_3OH**)]$^+$ (Figure S63). UV−vis, λ_{max} (nm), (ε (dm^3 mol^{-1}cm^{-1})) in 1X PBS solution: 435 (6900), 348 (3400).

^{1}H NMR (DMSO-d_6, 300 MHz) δ ppm: 2.12 (−CH_3) (s, 6H), 3.60 (t, 8H, J_1 = J_2 = 3 Hz), 3.77 (−CH_2) (t, 4H, J_1 = J_2 = 3 Hz), 3.88(−CH_2) (s, 4H), 7.37 (Ar−H) (s, 2H), 7.77 (Ar−H) (s, 2H), 8.48 (−CH═N) (d, 4H, J = 9 Hz).

^{13}C NMR (DMSO-d_6, 300 MHz) δ ppm: 19.97, 21.55, 51.50, 55.68, 66.75, 67.07, 116.74, 119.26, 122.09, 125.25, 129.76, 137.90, 146.03, 154.54, 168.71, 172.55.

Synthesis of Complex (7) {[Cr(L2)](NO_3)}. A 5 mL methanolic solution of chromium nitrate nonahydrate (1.0 mmol, 0.400 g) was added dropwise to a 20 mL methanolic solution of **H_2L2** (1.0 mmol, 0.464 g). The resultant reaction mixture was stirred for ∼4 h. A dark green colored solid mass was obtained after evaporation of the solvent.

Yield: 0.416g (81%). Anal. Calc. for $C_{26}H_{30}N_5O_7Cr$: C 54.16%; H 5.24%; N 12.15%. Found: C 54.13%; H 5.22%; N 12.11%. IR (cm^{-1}, KBr): υ(C═N) 1639s; υ(NO_3^-)1330s. UV−vis, λ_{max} (nm), (ε (dm^3 mol^{-1}cm^{-1})) in 1X PBS solution: 435 (7150), 348 (3400).

UV−visible and Fluorescence Spectroscopic Studies. Stock solutions of the various ions (1 × 10^{-3} M) were prepared in deionized water. A stock solution of **H_2L1** and **H_2L2** (1 × 10^{-3} M) were prepared in MeOH medium. All the spectroscopic experiments including competitive assays of various cations and anions were performed in 1X PBS solution. In titration experiments, a 60 μL solution of (1 × 10^{-3} M) **H_2L1** and **H_2L2** was taken for 3000 μL in a quartz optical cell of 1.0 cm optical path length, and the corresponding metal stock solutions of the metal ions were gradually added to it, respectively.

Cell Culture. The HepG2 cells and WI38 were obtained from the National Center for Cell Science (NCCS) Pune, India. The cells were grown in DMEM with 10% FBS (Fetal Bovine Serum), penicillin/streptomycin (100 units/ml) at 37 °C and 5% CO_2. All the treatments were conducted at 37 °C and at a cell density allowing exponential growth.

Cell Imaging. The *HepG2* cells were grown in coverslips for 24 h. Then the cells were either mock-treated or treated with 10 μM of ligand **H_2L1** and **H_2L2**, Zn^{2+} salt (10 μM), Al^{3+} salt (10 μM), Cr^{3+} salt (10 μM) and Fe^{3+} salt (10 μM) for 24 h at 37 °C. The cells were washed with 1X PBS. Then they were mounted on a glass slide and observed under fluorescence microscope (Leica) with a filter having excitation of 450−500 nm (blue) and an emission of 500−570 nm (green).

Cell Survivability Assay. Cell survivability of **H_2L1** and **H_2L2** were studied for WI-38 (noncancerous cells), following reported procedure.[66] In brief, viability of these cells after exposure to various concentrations of ligand was assessed by MTT assay. The cells were seeded in 96-well plates at 1 × 10^4 cells per well and exposed to ligand at concentrations of 0 μM, 20 μM, 40 μM, 60 μM, 80 μM, 100 μM for 24 h. The resulting formazan crystals were dissolved in an MTT solubilization buffer and the absorbance was measured at 570 nm by using a spectrophotometer (BioTek) and the value was compared with control cells. The cell cytotoxicity of the complexes toward the WI-38 cell was envisaged following the above-mentioned MTT assay protocol.

■ ASSOCIATED CONTENT

Supporting Information

The Supporting Information is available free of charge at https://pubs.acs.org/doi/10.1021/acsomega.2c06549.

Crystallographic data for complex **1** (CIF)

Additional supplementary data as mentioned in the text (PDF)

https://doi.org/10.1021/acsomega.2c06549
ACS Omega 2023, 8, 7479−7491

AUTHOR INFORMATION

Corresponding Author

Amrita Saha − *Department of Chemistry, Jadavpur University, Kolkata 700032, India;* orcid.org/0000-0001-9357-801X; Phone: +91-33-24572146; Email: amritasahachemju@gmail.com

Authors

Mohafuza Khatun − *Department of Chemistry, Jadavpur University, Kolkata 700032, India*

Pravat Ghorai − *Department of Chemistry, Jadavpur University, Kolkata 700032, India*

Jayanta Mandal − *Department of Chemistry, Jadavpur University, Kolkata 700032, India*

Sougata Ghosh Chowdhury − *Department of Life Science and Biotechnology, Jadavpur University, Kolkata 700032, India*

Parimal Karmakar − *Department of Life Science and Biotechnology, Jadavpur University, Kolkata 700032, India*

Salvador Blasco − *Institute of Molecular Sciences, Universitat de València, Paterna, Valencia 46980, Spain;* orcid.org/0000-0002-8142-8337

Enrique García-España − *Institute of Molecular Sciences, Universitat de València, Paterna, Valencia 46980, Spain;* orcid.org/0000-0002-4601-6505

Complete contact information is available at: https://pubs.acs.org/10.1021/acsomega.2c06549

Notes

The authors declare no competing financial interest.

ACKNOWLEDGMENTS

A.S. gratefully acknowledges the financial support of this work by the DST, India (Sanction No. SB/FT/CS-102/2014, dated-18.07.2015), and RUSA 2.0, Government of India (Sanction No. R-11/262/19, dated March 08, 2019). P. G. heartily acknowledges the CSIR, Government of India (File no. 09/096(1019)/2020 EMR-I) for his fellowship.

REFERENCES

(1) Carter, K. P.; Young, A. M.; Palmer, A. E. Fluorescent Sensors for Measuring Metal Ions in Living Systems. *Chem. Rev.* **2014**, *114*, 4564−4601.

(2) McKee, T.; McKee, J. R. *Biochemistry: An Introduction*, 2nd ed.; McGraw-Hill Companies, Inc.: New York, 1999.

(3) Mathews, C. K.; Van Holde, K. E. *Biochemistry*, 2nd ed; The Benjamin/Cummings Publishing Company, Inc.: Menlo Park, 1996.

(4) Bonnet, C. S.; Toth, E. MRI probes for sensing biologically relevant metal ions. *Future Med. Chem.* **2010**, *2*, 367−384.

(5) Tsien, R. Y. *Fluorescent and Photochemical Probes of Dynamic Biochemical Signals inside Living Cells*; Czarnik, A. W., Ed.; American Chemical Society: Washington DC, 1993.

(6) (a) Schmittel, M.; Lin, H.-W. Quadruple-Channel Sensing: A Molecular Sensor with a Single Type of Receptor Site for Selective and Quantitative Multi-Ion Analysis. *Angew. Chem., Int. Ed.* **2007**, *46*, 893−896. (b) Basa, P. N.; Sykes, A. G. J. Differential sensing of Zn(II) and Cu(II) via two independent mechanisms. *Org.Chem.* **2012**, *77*, 8428−8434. (c) Zhang, J. F.; Zhou, Y.; Yoon, J.; Kim, Y.; Kim, S. J.; Kim, J. S. Naphthalimide Modified Rhodamine Derivative: Ratiometric and Selective Fluorescent Sensor for Cu^{2+} Based on Two Different Approaches. *Org. Lett.* **2010**, *12*, 3852−3855. (d) Maity, D.; Govindaraju, T. A differentially selective sensor with fluorescence turn-on response to Zn^{2+} and dual-mode ratiometric response to Al^{3+} in aqueous media. *Chem.Commun.* **2012**, *48*, 1039−1041. (e) Kaur, N.; Kumar, S. Single molecular colorimetric probe for simultaneous estimation of Cu^{2+} and Ni^{2+}. *Chem. Commun.* **2007**, 3069−3070. (f) Luxami, V.; Kumar, S. ESIPT based dual fluorescent sensor and concentration dependent reconfigurable boolean operators. *RSC Adv.* **2012**, *2*, 8734−8740. (g) Wang, L.; Yan, J.; Qin, W.; Liu, W.; Wang, R. A new rhodamine-based single molecule multi analyte (Cu^{2+}, Hg^{2+}) sensor and its application in the biological system. *Dyes Pigm.* **2012**, *92*, 1083−1090.

(7) Wang, J.; Li, Y.; Patel, N. G.; Zhang, G.; Zhou, D.; Pang, Y. A single molecular probe for multi-analyte (Cr^{3+}, Al^{3+} and Fe^{3+}) detection in aqueous medium and its biological application. *Chem. Commun.* **2014**, *50*, 12258−12261.

(8) Paul, S.; Manna, A.; Goswami, S. A differentially selective molecular probe for detection of trivalent ions (Al^{3+}, Cr^{3+} and Fe^{3+}) upon single excitation in mixed aqueous medium. *Dalton Trans.* **2015**, *44*, 11805−11810.

(9) Liu, Y.; Wang, D.; Zheng, X. J.; Jin, L. P. Binding site-driven sensing properties of a quinazoline derivative with metal cations. *RSC Adv.* **2015**, *5*, 36987−36992.

(10) Shellaiah, M.; Simon, T.; Srinivasadesikan, V.; Lin, C. M.; Sun, K. W.; Ko, F. H.; Lin, M. C.; Lin, H. C. Novel pyrene containing monomeric and dimeric supramolecular AIEE active nano-probes utilized in selective "off−on" trivalent metal and highly acidic pH sensing with live cell applications. *J. Mater. Chem. C* **2016**, *4*, 2056−2071.

(11) Das, D.; Alam, R.; Katarkar, A.; Ali, M. A differentially selective probe for trivalent chemosensor upon single excitation with cell imaging application: potential applications in combinatorial logic circuit and memory devices. *Photochem.Photobiol. Sci.* **2019**, *18*, 242−252.

(12) Chandra, R.; Manna, A. K.; Rout, K.; Mondal, J.; Patra, G. K. A dipodal molecular probe for naked eye detection of trivalent cations (Al^{3+}, Fe^{3+} and Cr^{3+}) in aqueous medium and its applications in real sample analysis and molecular logic gates. *RSC Adv.* **2018**, *8*, 35946−35958.

(13) Janakipriya, S.; Chereddy, N. R.; Korrapati, P.; Thennarasu, S.; Mandal, A. B. Selective interactions of trivalent cations Fe^{3+}, Al^{3+} and Cr^{3+} turn on fluorescence in a naphthalimide based single molecular probe. *Spectrochimica acta.* **2016**, *153*, 465−470.

(14) Singha, D.; Das, T.; Satyanarayana, L.; Roy, P.; Nandi, M. Rhodamine functionalized mesoporous silica as a chemosensor for the efficient sensing of Al^{3+}, Cr^{3+} and Fe^{3+} ions and their removal from aqueous media. *New J. Chem.* **2019**, *43*, 15563−15574.

(15) Wang, J.; Li, Y.; Patel, N. G.; Zhang, G.; Zhou, D.; Pang, Y. A single molecular probe for multi-analyte (Cr^{3+}, Al^{3+} and Fe^{3+}) detection in aqueous medium and its biological application. *Chem. Commun.* **2014**, *50*, 12258−12261.

(16) (a) Ghorai, P.; Pal, K.; Karmakar, P.; Saha, A. The development of two fluorescent chemosensors for the selective detection of Zn^{2+} and Al^{3+} ions in a quinoline platform by tuning the substituents in the receptor part: elucidation of the structures of the metal-bound chemosensors and biological studies. *Dalton Trans.* **2020**, *49*, 4758−4773. (b) Mandal, J.; Pal, K.; Ghosh Chowdhury, S.; Karmakar, P.; Panja, A.; Banerjee, S.; Saha, A. Rhodamine-azo based two fluorescent probes for recognition of trivalent metal ions: crystal structures elucidation and biological application. *Dalton Trans.* **2022**, *51*, 15555.

(17) Trusso Sfrazzetto, G.; Satriano, C.; Tomaselli, G. A.; Rizzarelli, E. Synthetic fluorescent probes to map metallostasis and intracellular fate of zinc and copper. *Coord. Chem. Rev.* **2016**, *311*, 125−167.

(18) (a) D'Autréaux, B.; Tucker, N. P.; Dixon, R.; Spiro, S. A non-haem iron centre in the transcription factor NorR senses nitric oxide. *Nature* **2005**, *437*, 769−772. (b) Ercal, N.; Gurer-Orhan, H.; Aykin-Burns, N. Toxic metals and oxidative stress part I: mechanisms involved in metal-induced oxidative damage. *Curr. Top. Med. Chem.* **2001**, *1*, 529−539. (c) Wang, J.; Pantopoulos, K. Regulation of cellular iron metabolism. *Biochem. J.* **2011**, *434*, 365−381.

(19) Berg, J. M.; Godwin, H. A. Lessons from Zinc- Binding Peptides. *Annu. Rev. Biophys. Biomol. Struct.* **1997**, *26*, 357−371.

(20) Pithadia, A. S; Lim, M. H. Metal-associated amyloid-b species in Alzheimer's disease. *Curr. Opin. Chem. Biol.* **2012**, *16*, 67−73.

(21) Vincent, J. B. New Evidence against Chromium as an Essential Trace Element. *Journal of Nutrition* **2017**, *147*, 2212−2219.
(22) Stearns, D. M. Is chromium a trace essential metal? *BioFactors* **2000**, *11*, 149−162.
(23) Bondy, S. C. The neurotoxicity of environmental aluminum is still an issue. *Neurotoxicology.* **2010**, *31*, 575−581.
(24) Fasman, G. D. Aluminum and Alzheimer's disease: model studies. *Coord. Chem. Rev.* **1996**, *149*, 125−165.
(25) Perl, D. P.; Gajdusek, D. C.; Garruto, R. M.; Yanagihara, R. T.; Gibbs, C. J. Intraneuronal aluminum accumulation in amyotrophic lateral sclerosis and Parkinsonism-dementia of Guam. *Science.* **1982**, *217*, 1053−1055.
(26) Park, S. H.; Kwon, N.; Lee, J. H.; Yoon, J.; Shin, I. Synthetic ratiometric fluorescent probes for detection of ions. *Chem. Soc. Rev.* **2020**, *49*, 143−179.
(27) Zhu, H.; Fan, J.; Wang, B.; Peng, X. Fluorescent, MRI, and colorimetric chemical sensors for the first-row d-block metal ions. *Chem. Soc. Rev.* **2015**, *44*, 4337−4366.
(28) Wu, D.; Sedgwick, A. C.; Gunnlaugsson, T.; Akkaya, E. U.; Yoon, J.; James, T. D. Fluorescent chemosensors: the past, present and future. *Chem. Soc. Rev.* **2017**, *46*, 7105−7123.
(29) Sedgwick, A. C.; Wu, L.; Han, H. H.; Bull, S. D.; He, X. P.; James, T. D.; Sessler, J. L.; Tang, B. Z.; Tian, H.; Yoon, J. Excited-state intramolecular proton-transfer (ESIPT) based fluorescence sensors and imaging agents. *Chem. Soc. Rev.* **2018**, *47*, 8842−8880.
(30) Wu, L.; Huang, C.; Emery, B. P.; Sedgwick, A. C.; Bull, S. D.; He, X. P.; Tian, H.; Yoon, J.; Sessler, J. L.; James, T. D. Forster resonance energy transfer (FRET)-based small-molecule sensors and imaging agents. *Chem. Soc. Rev.* **2020**, *49*, 5110−5139.
(31) Lu, Y.; Huang, S.; Liu, Y.; He, S.; Zhao, L.; Zeng, X. Highly Selective and Sensitive Fluorescent Turn-on Chemosensor for Al^{3+} Based on a Novel Photoinduced Electron Transfer Approach. *Org. Lett.* **2011**, *13*, 5274−5277.
(32) (a) Tachapermpon, Y.; Thavornpradit, S.; Charoenpanich, A.; Sirirak, J.; Burgess, K.; Wanichacheva, N. Near-infrared aza-BODIPY fluorescent probe for selective Cu^{2+} detection and its potential in living cell imaging. *Dalton Trans.* **2017**, *46*, 16251−16256. (b) Liu, T.; Dong, Y.; Wan, X.; Li, W.; Yao, Y. An easy and accessible water-soluble sensor for the distinctive fluorescence detection of Zn^{2+} and Al^{3+} ions. *RSC Adv.* **2015**, *5*, 76939−76942.
(33) (a) Hou, L.; Feng, J.; Wang, Y.; Dong, C.; Shuang, S.; Wang, Y. Single fluorescein-based probe for selective colorimetric and fluorometric dual sensing of Al^{3+} and Cu^{2+}. *Sens. Actuators B* **2017**, *247*, 451−460. (b) Qin, J. -c.; Fan, L.; Wang, B. -d.; Yang, Z. -y.; Li, T. -r. The design of a simple fluorescent chemosensor for Al^{3+}/Zn^{2+} via two different approaches. *Anal. Methods.* **2015**, *7*, 716−722.
(34) Chen, X.; Pradhan, T.; Wang, F.; Kim, J. S.; Yoon, J. Fluorescent Chemosensors Based on Spiro ring-Opening of Xanthenes and Related Derivatives. *Chem. Rev.* **2012**, *112*, 1910−1956.
(35) Kim, H. N.; Lee, M. H.; Kim, H. J.; Kim, J. S.; Yoon, J. A new trend in rhodamine-based chemosensors: application of spirolactam ring-opening to sensing ions. *Chem. Soc. Rev.* **2008**, *37*, 1465−1472.
(36) Dujols, V.; Ford, F.; Czarnik, A. W. A Long-Wavelength Fluorescent Chemodosimeter Selective for Cu(II) Ion in Water. *J. Am. Chem. Soc.* **1997**, *119*, 7386−7387.
(37) Quang, D. T.; Kim, J. S. Fluoro- and Chromogenic Chemodosimeters for Heavy Metal Ion Detection in Solution and Biospecimens. *Chem. Rev.* **2010**, *110*, 6280−6301.
(38) Wong, B. A.; Friedle, S.; Lippard, S. J. Solution and Fluorescence Properties of Symmetric Dipicolylamine-Containing Dichlorofluorescein-Based Zn^{2+} Sensors. *J. Am. Chem. Soc.* **2009**, *131*, 7142−7152.
(39) Zhang, X.; Hayes, D.; Smith, S. J.; Friedle, S.; Lippard, S. J. New Strategy for Quantifying Biological Zinc by a Modified Zinpyr Fluorescence Sensor. *J. Am. Chem. Soc.* **2008**, *130*, 15788−15789.
(40) Xue, L.; Li, G.; Zhu, D.; Liu, Q.; Jiang, H. Rational Design of a Ratiometric and Targetable Fluorescent Probe for Imaging Lysosomal Zinc Ions. *Inorg. Chem.* **2012**, *51*, 10842−10849.
(41) Xue, L.; Liu, Q.; Jiang, H. Ratiometric Zn^{2+} Fluorescent Sensor and New Approach for Sensing Cd^{2+} by Ratiometric Displacement. *Org. Lett.* **2009**, *11*, 3454−3457.
(42) Liu, H.; Dong, Y.; Zhang, B.; Liu, F.; Tan, C.; Tan, Y.; Jiang, Y. An efficient quinoline based fluorescence sensor for zinc (II) and its application in live-cell imaging. *Sens. Actuators B* **2016**, *234*, 616−624.
(43) Xu, Z.; Yoon, J.; Spring, D. R. Fluorescent chemosensors for Zn^{2+}. *Chem. Soc. Rev.* **2010**, *39*, 1996−2006.
(44) Fu, Y.; Fan, C.; Liu, G.; Cui, S.; Pu, S. A highly selective and sensitive ratiometric fluorescent chemosensor for Zn^{2+} based on diarylethene with a benzyl-linked 8-aminoquinoline-2-aminomethylpyridine unit. *Dyes Pigm.* **2016**, *126*, 121−130.
(45) (a) Zhang, Y.; Guo, X.; Si, W.; Jia, L.; Qian, X. Ratiometric and Water-Soluble Fluorescent Zinc Sensor of Carboxamidoquinoline with an Alkoxyethylamino Chain as Receptor. *Org. Lett.* **2008**, *10*, 473−476. (b) He, C.; Lin, Z.; He, Z.; Duan, C.; Xu, C.; Wang, Z.; Yan, C. Metal-Tunable Nanocages as Artificial Chemosensors. *Angew. Chem., Int. Ed.* **2008**, *47*, 877−881.
(46) Ravikumar, I.; Ghosh, P. Zinc(II) and PPi Selective Fluorescence OFF-ON-OFF Functionality of a Chemosensor in Physiological Conditions. *Inorg. Chem.* **2011**, *50*, 4229−4231.
(47) Maity, D.; Govindaraju, T. A differentially selective sensor with fluorescence turn-on response to Zn^{2+} and dual-mode ratiometric response to Al^{3+} in aqueous media. *Chem. Commun.* **2012**, *48*, 1039−1041.
(48) (a) Ma, C. T. L.; MacLachlan, M. J. Supramolecular Assembly and Coordination Assisted Deaggregation of MultimetallicMacrocycles. *Angew.Chem. Int. Ed.* **2005**, *44*, 4178−4182. (b) Huang, W.; Zhu, H. B.; Gou, S. H. Self-assembly directed by dinuclear zinc(II) macrocyclic species. *Coord. Chem. Rev.* **2006**, *250*, 414−423. (c) Anbu, S.; Kandaswamy, M.; Suthakaran, P.; Murugan, V.; Varghese, B. Structural, magnetic, electrochemical, catalytic, DNA binding and cleavage studies of new macrocyclic binuclear copper(II) complexes. *J. Inorg. Biochem.* **2009**, *103*, 401−410. (d) Singh, D. P.; Kumar, K.; Sharma, C. Antimicrobial active macrocyclic complexes of Cr(III), Mn(III) and Fe(III) with their spectroscopic approach. *Eur. J. Med. Chem.* **2009**, *44*, 3299−3304. (e) Hui, J. K.; Frischmann, P. D.; Tso, C. H.; Michal, C. A.; Maclachlan, M. J. Spontaneous Hierarchical Assembly of Crown Ether-like Macrocycles into Nanofibers and Microfibers Induced by Alkali-Metal and Ammonium Salts. *Chem. − Eur. J.* **2010**, *16*, 2453−2460. (f) Janczak, J.; Prochowicz, D.; Lewinski, J.; Fairen-Jimenez, D.; Bereta, T.; Lisowski, J. Trinuclear Cage-Like Zn^{II} Macrocyclic Complexes: Enantiomeric Recognition and Gas Adsorption Properties. *Chem.−Eur. J.* **2016**, *22*, 598−609. (g) Matsunaga, S.; Shibasaki, M. Recent advances in cooperative bimetallic asymmetric catalysis: dinuclear Schiff base complexes. *Chem. Commun.* **2014**, *50*, 1044−1057. (h) Vallee, B. L.; Williams, R. J. P. Metalloenzymes: the entatic nature of their active sites. *Proc. Natl. Acad. Sci. U.S.A.* **1968**, *59*, 498−505.
(49) (a) Qin, Y.; Liu, X.; Jia, P. P.; Xu, L.; Yang, H. B. BODIPY-based macrocycles. *Chem. Soc. Rev.* **2020**, *49*, 5678−5703. (b) Ghorai, P.; Ghosh Chowdhury, S.; Pal, K.; Mandal, J.; Karmakar, P.; Franconetti, A.; Frontera, A.; Blasco, S.; Garcia-Espana, E.; Parui, P. P.; Saha, A. Aza-Crown-Based Macrocyclic Probe Design for "PET-off" Multi-Cu2+ Responsive and "CHEF-on" Multi-Zn2+ Sensor: Application in Biological Cell Imaging and Theoretical Studies. *Inorg. Chem.* **2022**, *61*, 1982−1996. (c) Pina, F.; Bernardo, M. A.; García-España, E. Fluorescent Chemosensors Containing Polyamine Receptors. *Eur. J. Inorg. Chem.* **2000**, *2000*, 2143−2157. (d) Martínez-Manez, R.; Sancenon, F. Fluorogenic and Chromogenic Chemosensors and Reagents for Anions. *Chem. Rev.* **2003**, *103*, 4419−4476. (e) Verdejo, B.; Inclán, M.; Clares, M. P.; Bonastre-Sabater, I.; Ruiz-Gasent, M.; García-España, E. Fluorescent Chemosensors Based on Polyamine Ligands: A Review. *Chemosensors* **2022**, *10*, 1. (f) Pla, L.; Lozano-Torres, B.; Martínez-Máñez, R.; Sancenón, F.; Ros-Lis, J. V. Overview of the Evolution of Silica-Based Chromo-Fluorogenic Nanosensors. *Sensors* **2019**, *19*, 5138.
(50) Nepogodiev, S. A.; Stoddart, J. F. Cyclodextrin-Based Catenanes and Rotaxanes. *Chem. Rev.* **1998**, *98*, 1959−1976.

https://doi.org/10.1021/acsomega.2c06549
ACS Omega 2023, 8, 7479−7491

(51) Ji, X.; Chi, X.; Ahmed, M.; Long, L.; Sessler, J. L. Soft Materials Constructed Using Calix[4] pyrrole- and "Texas-Sized" Box-Based Anion Receptors. *Acc. Chem. Res.* **2019**, *52*, 1915−1927.
(52) Jie, K.; Zhou, Y.; Li, E.; Huang, F. Nonporous Adaptive Crystals of Pillararenes. *Acc. Chem. Res.* **2018**, *51*, 2064−2072.
(53) Bianchi, A.; García-España, E. Azacycloalkanes and Azacyclophanes. *Supramolecular Chemistry: From Molecules to Nanomaterials*; John Wiley & Sons, Ltd., 2012. DOI: 10.1002/9780470661345.smc048.
(54) (a) Okawa, H.; Furutachi, H.; Fenton, D. E. Heterodinuclear metal complexes of phenol-based compartmental macrocycles. *Coord. Chem. Rev.* **1998**, *174*, 51−75. (b) Fraser, C.; Johnston, L.; Rheingold, A. L.; Haggerty, B. S.; Williams, G. K.; Whelan, J.; Bosnich, B. Bimetallic Reactivity. Synthesis, Structure and Reactivity of Homo- and Heterobimetallic Complexes of a Binucleating Macrocyclic Ligand Containing 6- and 4-Coordination Sites. *Inorg. Chem.* **1992**, *31*, 1835−1844. (c) McCollum, D. G.; Yap, G. P. A.; Rheingold, A. L.; Bosnich, B. Bimetallic Reactivity. Synthesis of Bimetallic Complexes of Macrocyclic Binucleating Ligands Containing 6- and 4-Coordinate Sites and Their Reactivity with Dioxygen and Other Oxidants. *J. Am. Chem. Soc.* **1996**, *118*, 1365−1379. (d) Karunakaran, S.; Kandaswamy, M. Synthesis, Electrochemical and Magnetic Properties of New Acyclic 'Side-off ' Binuclear Copper(II) Complexes. *J. Chem. Soc., Dalton Trans.* **1994**, 1595−1599. (e) Rybak-Akimova, E. V.; Alcock, N. W.; Busch, D. H. Dicompartmental Ligands with Hexa- and Tetradentate Coordination Sites: One-Step Synthesis of Ligands and Metal Complexes and Their X-ray Structure Analysis. *Inorg. Chem.* **1998**, *37*, 1563−1574.
(55) (a) Yonemura, M.; Matsumura, Y.; Furutachi, H.; Ohba, M.; Okawa, H.; Fenton, D. E. Migratory Transmetalation in Diphenoxo-Bridged Cu″M″ Complexes of a Dinucleating Macrocycle with $N(amine)_2$ O_2 and $N(imine)_2$ O_2 Metal-Binding Sites. *Inorg. Chem.* **1997**, *36*, 2711−2717. (b) Yonemura, M.; Ohba, M.; Takahashi, K.; Okawa, H.; Fenton, D. E. Dinuclear Cu″M″ complexes of a phenol-based macrocycle with N $(amine)_2$ O_2 and N $(imine)_2O_2$ metal-binding sites: the effect of chloride ligation upon the site selectivity of metal ions. *Inorg. Chim. Acta* **1998**, *283*, 72−79.
(56) (a) Yonemura, M.; Nakamura, Y.; Usuki, N.; Okawa, H. Macrocyclic effects upon isomeric Cu″M″ or M″Cu″ cores. Formation with unsymmetric phenol-based macrocyclic ligands. *Proc. Ind. Acad. Sci.(Chem. Ser.).* **2000**, *112*, 291−310. (b) Yonemura, M.; Usuki, N.; Nakamura, Y.; Ohba, M.; Okawa, H. Macrocyclic effect upon site-selective Cu″M″ or M″Cu″ core formation with unsymmetric phenol-based macrocyclic ligands. *J. Chem. Soc., Dalton Trans.* **2000**, 3624−3631. (c) Yonemura, M.; Arimura, K.; Inoue, K.; Usuki, N.; Ohba, M.; Okawa, H. Coordination-Position Isomeric M″Cu″ and Cu″M″ (M = Co, Ni, Zn) Complexes Derived from Macrocyclic Compartmental Ligands. *Inorg.Chem.* **2002**, *41*, 582−589.
(57) (a) Wang, Z.; Martell, A. E.; Motekaitis, R. J.; Reibenspies, J. H. The first systematic stability study of mononuclear and dinuclear iron(II) and iron(III) complexes incorporating a dinucleating macrocyclic ligand in aqueous solution. *J. Chem. Soc., Dalton Trans.* **1999**, 2441−2449. (b) Shangguan, G. Q.; Martell, A. E.; Zhang, Z. R.; Reibenspies, J. The synthesis, crystal structure and metal complexes of a new macrocyclic dinucleating ligand, 3,6,9,17,20,23-hexaaza-29,30-dihydroxy-13,27-dimethyltricyclo[23,3,1,$1^{11,15}$]triaconta1-(28),11,13,15(30),25,26-hexaene. *Inorg. Chim. Acta* **2000**, *299*, 47−58. (c) Kong, D. Y.; Martell, A. E.; Motekaitis, R. J. Studies on 24-Membered Macrocyclic Mononuclear and Dinuclear Iron Complexes: Stability and Catalytic Hydroxylation of Adamantane by Divalent Iron Complexes. *Ind. Eng. Chem. Res.* **2000**, *39*, 3429−3435. (d) Kong, D.; Reibenspies, J.; Martell, A. E.; Motekaitis, R. J. A new unsymmetrical polyamine macrocycle incorporating two phenolic functions: synthesis, basicity and coordination behavior toward copper(II). *Inorg. Chim. Acta* **2001**, *324*, 35−45. (e) Wang, J.; Martell, A. E.; Motikatis, R. J. The synthesis crystal structure and complexation of a new octacoordinatehexaazamacrocyclic ligand. *Inorg. Chim. Acta* **2001**, *322*, 47−55. (f) Wang, J.; Kong, D.; Martell, A. E; Motekatis, R. J; Reibenspies, J. H Complexation of Cu(II)M(II) (M = Cd, Co, Ni, Zn) heterodinuclear compounds of an octa coordinate hexaazamacrocyclic ligand. *Inorg. Chim. Acta* **2001**, *324*, 194−202. (g) Gao, J.; Martell, A. E.; Motekaitis, R. J. Novel macrocyclic hetero dinuclear catalase-like model complex CuMnL and CuZnL (L = BDBPH): synthesis, stability and catalytic properties. *Inorg. Chim. Acta* **2001**, *325*, 164−170. (h) Kong, D. Y.; Martell, A. E.; Reibenspies, J. H. Macrocyclic dinuclear Zn(II) complexes: synthesis, structure and hydrolysis of tris(p-nitrophenyl) phosphate. *Inorg. Chim. Acta* **2002**, *333*, 7−14. (i) Kong, D.; Reibenspies, J.; Mao, J.; Clearfield, A.; Martell, A. E. Novel 30-membered octa aza macrocyclic ligand: synthesis, characterization, thermodynamic stabilities and DNA cleavage activity of homodinuclear copper and nickel complexes. *Inorg. Chim. Acta* **2003**, *342*, 158−170.
(58) (a) Ambrosi, G.; Micheloni, M.; Paderni, D.; Formica, M.; Giorgi, L.; Fusi, V. Fluorescent macrocyclic chemosensor for Zn(II) detection at alkaline pH values. *Supramol. Chem.* **2020**, *32*, 139−149. (b) Ghanbari, B.; Zarepour-jevinani, M. Promotional effect of macrocyclization in O_2N_x naphtha-aza-crown macrocyclic ligands on fluorescence chemosensing of Al(III). *J. Lumin.* **2019**, *205*, 219−227. (c) Goswami, S.; Maity, S.; Maity, A. C.; Das, A. K.; Khanra, K.; Mandal, T. K.; Bhattacharyya, N. A macrocyclic piperazine linked extremely Zn^{2+} selective fluorescent chemosensor with bio-imaging and for $H_2PO_4^-$ sensing. *Tetrahedron Lett.* **2014**, *55*, 5993−5997. (d) Bhanja, A. K.; Patra, C.; Mondal, S.; Mishra, S.; Saha, K. D.; Sinha, C. Macrocycle aza-crown chromogenic reagent to Al^{3+} and fluorescence sensor for Zn^{2+} and Al^{3+} along with live cell application and logic operation. *Sens. Actuators, B* **2017**, *252*, 257−267. (e) Kumar, B. S.; Chandra, B.; Jovan Jose, K. V.; Panda, P. K. 1,2-Phenylene-Incorporated Smallest Expanded Calix[4]pyrrole via One-Step Synthesis of Tetrapyrrane: A Fluorescent Host for Fluoride Ion. *J. Org. Chem.* **2021**, *86*, 10536−10543. (f) Azadbakht, R.; Chehri, N. A new fluorescent macrocyclic nano-chemosensor for Fe^{3+} and I^- in aqueous solution. *New J. Chem.* **2018**, *42*, 17690−17699. (g) Das, S.; Adhikary, J.; Chakraborty, P.; Chakraborty, T.; Das, D. Macrocyclization of N, N0-propylenebis(3-formyl-5-tert-butylsalicylaldimine): a ratiometric fluorescence chemodosimeter for Zn^{II}. *RSC Adv.* **2016**, *6*, 98620−98631. (h) Paderni, D.; Giorgi, L.; Voccia, M.; Formica, M.; Caporaso, L.; Macedi, E.; Fusi, V. A New Benzoxazole-Based Fluorescent Macrocyclic Chemosensor for Optical Detection of Zn^{2+} and Cd^{2+}. *Chemosensors* **2022**, *10*, 188−205. (i) Patra, S.; Boricha, V. P.; Paul, P. Dual-Mode Calixarene-Based Chemosensor: Highly Selective Fluorogenic Detection of Hg^{2+} and Chromogenic Detection of Cu^{2+} with a Single Ionophore. *Eur. J. Inorg. Chem.* **2019**, *2019*, 199−205.
(59) Gagne, R. R.; Spiro, C. L.; Smith, T. J.; Hamann, C. A.; Thies, W. R.; Shiemke, A. D. The Synthesis, Redox Properties and Ligand Binding of Heterobinuclear Transition-Metal Macrocyclic Ligand Complexes. Measurement of an Apparent Delocalization Energy in a Mixed-Valent $Cu^{I}Cu^{II}$ Complex. *J. Am. Chem. Soc.* **1981**, *103*, 4073−4081.
(60) (a) Benesi, H. A.; Hildebrand, J. H. A Spectrophotometric Investigation of the Interaction of Iodine with Aromatic Hydrocarbons. *J. Am. Chem. Soc.* **1949**, *71*, 2703−2707. (b) Gans, P.; Sabatini, A.; Vacca, A. Determination of Equilibrium Constants from Spectrophotometric Data obtained from Solutions of known pH: The Program pHab. *Annali di Chimica* **1999**, *89*, 45−49. (c) Alderighi, L.; Gans, P.; Ienco, A.; Peters, D.; Sabatini, A.; Vacca, A. Hyperquad simulation and speciation (HySS): a utility program for the investigation of equilibria involving soluble and partially soluble species. *Coord. Chem. Rev.* **1999**, *184*, 311−318.
(61) (a) Tang, B.; Wu, T. J.; Dong, Y.; Ding, Y.; Wang, H. Rapid and sensitive spectrofluorimetric determination of trace amount of Cr(III) with o-vanillin-8-aminoquinoline. *Talanta* **2004**, *64*, 955−960. (b) Chang, J. H.; Choi, Y. M.; Shin, Y. K. A Significant Fluorescence Quenching of Anthrylaminobenzocrown Ethers by Paramagnetic Metal Cations. *Bull. Korean Chem. Soc.* **2001**, *22*, 527−530. (c) Nolan, E. M.; Jaworski, J.; Racine, M. E.; Sheng, M.; Lippard, S. J. Midrange Affinity Fluorescent Zn(II) Sensors of the Zinpyr Family: Syntheses,

Characterization, and Biological Imaging Applications. *Inorg. Chem.* **2006**, *45*, 9748−9757. (d) Wu, D. Y.; Xie, L. X.; Zhang, C. L.; Duan, C. Y.; Zhao, Y. G.; Guo, Z. J. Quinoline-based molecular clips for selective fluorescent detection of Zn^{2+}. *Dalton Trans.* **2006**, 3528−3533. (e) Wu, D. Y.; Huang, W.; Duan, C. Y.; Lin, Z. H.; Meng, Q. J. Highly Sensitive Fluorescent Probe for Selective Detection of Hg^{2+} in DMF Aqueous Media. *Inorg. Chem.* **2007**, *46*, 1538−1540. (f) Mao, J.; Wang, L. N.; Dou, W.; Tang, X. L.; Yan, Y.; Liu, W. S. Tuning the Selectivity of Two Chemosensors to Fe(III) and Cr(III). *Org. Lett.* **2007**, *9*, 4567−4570. (g) Huang, K.; Yang, H.; Zhou, Z.; Yu, M.; Li, F.; Gao, X.; Yi, T.; Huang, C. Multi signal Chemosensor for Cr^{3+} and Its Application in Bioimaging. *Org. Lett.* **2008**, *10*, 2557−2560. (h) Zhou, Z.; Yu, M.; Yang, H.; Huang, K.; Li, F.; Yi, T.; Huang, C. FRET-based sensor for imaging chromium(III) in living cells. *Chem. Commun.* **2008**, 3387−3389. (i) Aoki, S.; Kagata, D.; Shiro, M.; Takeda, K.; Kimura, E. Metal Chelation-Controlled Twisted Intramolecular Charge Transfer and Its Application to Fluorescent Sensing of Metal Ions and Anions. *J. Am. Chem. Soc.* **2004**, *126*, 13377−13390. (j) Maity, D.; Govindaraju, T. Naphthaldehyde−Urea/Thiourea Conjugates as Turn-On Fluorescent Probes for Al^{3+} Based on Restricted C═N Isomerization. *E. J. of Inorganic Chemistry* **2011**, *2011*, 5479−5485. (k) Wu, J. S.; Liu, W. M.; Zhuang, X. Q.; Wang, F.; Wang, P. F.; Tao, S. L.; Zhang, X. H.; Wu, S. K.; Lee, S. T. Fluorescence turn on of coumarin derivatives by metal cations: a new signaling mechanism based on C═N isomerization. *Org. Lett.* **2007**, *9*, 33−36. (l) Jung, H. S.; Ko, K. C.; Lee, J. H.; Kim, S. H.; Bhuniya, S.; Lee, J. Y.; Kim, Y.; Kim, S. J.; Kim, J. S. Rationally designed fluorescence turn-on sensors: A new design strategy based on orbital control. *Inorg. Chem.* **2010**, *49*, 8552−8557.

(62) Pradhan, A. B.; Mandal, S. K.; Banerjee, S.; Mukherjee, A.; Das, S.; Bukhsh, A. R. K.; Saha, A. A highly selective fluorescent sensor for zinc ion based on quinoline platform with potential applications for cell imaging studies. *Polyhedron* **2015**, *94*, 75−82.

(63) Sheldrick, G. M. *SAINT, Version 6.02, SADABS, Version 2.03*; Bruker AXS Inc.: Madison, WI, 2002.

(64) Sheldrick, G. M. *SADABS: Software for Empirical Absorption Correction*; University of Gottingen, Institute fur Anorganische Chemieder Universitat: Gottingen, Germany, 1999−2003.

(65) Sheldrick, G. M. Crystal structure refinement with SHELXL. *Acta Crystallogr.* **2015**, *C71*, 3−8.

(66) (a) Pramanik, A.; Laha, D.; Dash, S. K.; Chattopadhyay, S.; Roy, S.; Das, D. K.; Pramanik, P.; Karmakar, P. An in-vivo study for targeted delivery of copper-organic complex to breast cancer using chitosan polymer nanoparticles. *Materials Science and Engineering C* **2016**, *65*, 327−337. (b) Laha, D.; Pramanik, A.; Chattopadhyay, S.; Dash, S. K.; Roy, S.; Pramanik, P.; Karmakar, P. Folic acid modified copper oxide nanoparticles for targeted delivery in in vitro and in vivo systems. *RSC Adv.* **2015**, *5*, 68169−68178.

https://doi.org/10.1021/acsomega.2c06549
ACS Omega 2023, 8, 7479−7491